

Anthropogenic contributions to the 2021 Pacific Northwest heatwave

Emily Bercos-Hickey¹, Travis Allen O'Brien², Michael F Wehner³, Likun Zhang⁴, Christina M Patricola⁵, Huanping Huang¹, and Mark Risser¹

¹Lawrence Berkeley National Laboratory

²Indiana University Bloomington

³Lawrence Berkeley National Laboratory (DOE)

⁴University of Missouri

⁵Iowa State University

November 24, 2022

Abstract

Daily maximum temperatures during the 2021 heatwave in the Pacific Northwest United States and Canada shattered century old records. Multiple causal factors, including anthropogenic climate change, contributed to these high temperatures, challenging traditional methods of attributing human influence. We demonstrate that the observed 2021 daily maximum temperatures are far above the bounds of Generalized Extreme Value distributions fitted from historical data. Hence, confidence in Granger causal inference statements about the human influence on this heatwave is low. Alternatively, we present a more conditional hindcast attribution study using two regional models. We performed ensembles of simulations of the heatwave to investigate how the event would have changed if it had occurred without anthropogenic climate change and with future warming. We found that human activities caused a 1C increase in heatwave temperatures. Future warming would lead to a 5C increase in heatwave temperature by the end of the 21st century.

Abstract

Daily maximum temperatures during the 2021 heatwave in the Pacific Northwest United States and Canada shattered century old records. Multiple causal factors, including anthropogenic climate change, contributed to these high temperatures, challenging traditional methods of attributing human influence. We demonstrate that the observed 2021 daily maximum temperatures are far above the bounds of Generalized Extreme Value distributions fitted from historical data. Hence, confidence in Granger causal inference statements about the human influence on this heatwave is low. Alternatively, we present a more conditional hindcast attribution study using two regional models. We performed ensembles of simulations of the heatwave to investigate how the event would have changed if it had occurred without anthropogenic climate change and with future warming. We found that human activities caused a 1°C increase in heatwave temperatures. Future warming would lead to a 5°C increase in heatwave temperature by the end of the 21st century.

Plain Language Summary

While it is clear that global warming causes heatwaves to be warmer, the unique meteorological conditions behind the 2021 Pacific Northwest heatwave tax our ability to make quantitative estimates of the human contribution. We discuss why there is low confidence in traditional estimates of the human contribution to this heatwave's temperatures and present an alternative, albeit more highly constrained estimate that human activities caused a 1°C increase in the observed daily maximum temperatures. Additional future warming would lead to a 5°C increase in the heatwave by the end of the 21st century.

1 Introduction

On June 26–29, 2021, an unprecedented heatwave affected the Pacific Northwest (PNW) of the United States and western Canada. Temperature records were shattered, with all-time highs of 116°F (47°C) in Portland, Oregon, 108°F (42°C) in Seattle, Washington, and 121°F (49°C) in Lytton, British Columbia (Di Liberto, 2021). Heatwaves, characterized by prolonged periods of excessive heat, can have dangerous impacts on human health, infrastructure, and the environment (McEvoy et al., 2009; Perkins-Kirkpatrick & Alexander, 2013; Campbell et al., 2018; Ruffault et al., 2020), and the PNW heatwave was no exception. Over 500 deaths were attributed to the heatwave (Popovich & Choi-Schagrin, 2021), and the environment and infrastructure throughout the affected region were strained and damaged, with crops ruined and roads buckled due to the excessively hot temperatures (Baker & Sergio, 2021). The devastating and large-scale impacts of the PNW heatwave were exacerbated by the lack of adaptability of a region unaccustomed to such extreme high temperatures, with the observational record suggesting that this was a highly anomalous event (Figure 1).

The meteorological conditions of the PNW heatwave were similar to previous deadly heatwaves in Europe and Russia (Black et al., 2004; Dole et al., 2011). These events are associated with atmospheric blocking patterns, which are known to cause extreme heatwaves (Miralles et al., 2014; Horton et al., 2015; Schaller et al., 2018) and are characterized by a persistent, quasi-stationary, and often anticyclonic obstruction of the usual zonal flow (Rex, 1950; Sumner, 1954; Woollings et al., 2018). During the PNW heatwave, the high pressure of an omega block was centered over Washington and British Columbia (Figure S1) leading to subsidence and a multi-day period of hot, dry weather throughout the region (Neal et al., 2022). Additionally, an anomalous warm-season atmospheric river (AR) made landfall over the Alaska panhandle in late June and injected a large amount of moisture into western Canada and the PNW. The accumulation of water vapor under the high pressure of the atmospheric blocking pattern may have formed a positive

67 feedback loop that further enhanced the heatwave (Lin et al., 2022; Mo et al., 2022). These
68 two weather patterns were also superimposed on dry soil conditions, as 50% of Wash-
69 ington state and 70% of Oregon were in severe drought conditions in June 2021 (drought-
70 monitor.uni.edu).

71 The unprecedented nature of the PNW heatwave is also consistent with expecta-
72 tions from global warming (Perkins-Kirkpatrick & Gibson, 2017). Heatwaves have in-
73 creased since the 1950s (Perkins, 2015), and this observed increase in the frequency, in-
74 tensity, and duration of heatwaves has been attributed to anthropogenic climate change
75 (Meehl & Tebaldi, 2004; Diffenbaugh & Ashfaq, 2010; Perkins et al., 2012; Wuebbles et
76 al., 2014; Min et al., 2013; Wehner et al., 2018). The Intergovernmental Panel on Cli-
77 mate Change (IPCC) Sixth Assessment Report found that many heatwaves around the
78 world could be attributed to human influence (Seneviratne et al., 2021). Future warm-
79 ing will further increase the frequency, intensity, and duration of heat extremes (Vogel
80 et al., 2020), with the potential for temperatures to often reach dangerous levels for hu-
81 man health and agriculture (Sun et al., 2019).

82 The World Weather Attribution initiative (WWA, <https://www.worldweatherattribution.org/>)
83 performed analyses of the PNW heatwave within weeks of the event and made three rapid
84 attribution statements, which were later published (Philip et al., 2021). First, the ob-
85 served temperatures recorded were “virtually impossible” without anthropogenic climate
86 change. Second, after estimating that the observed temperatures had a return period of
87 approximately 1000 years, such annual maximum daily maximum temperatures (TXx)
88 “would have been at least 150 times rarer without human-induced climate change”. Third,
89 the heatwave was about 2°C warmer than it would have been without climate change
90 based on the change in 1000 year return values of TXx.

91 In this study, our objective is to revisit these rapid attribution statements and to
92 advance our understanding of how climate change affected the PNW heatwave. In sec-
93 tion 2, we discuss the limitations of statistical models to estimate the rarity of the PNW
94 heatwave. In section 3, we describe our experimental design of dynamical model simu-
95 lations of the PNW heatwave under past, present, and future climate conditions using
96 two regional climate models. In section 4, we discuss the resulting temperature changes
97 from these simulations. Finally, we present our conclusions in section 5.

98 2 Statistical modeling

99 Figure 1a shows maximum daily maximum temperatures between June 25 and July
100 4, 2021 from the Global Historical Climatology Network (GHCN) station data. Figure
101 1a reveals that most stations in this region had values greater than 45°C. Figure 1b com-
102 pares the summertime (June/July/August, JJA) TXx from all of the US stations within
103 the WWA region (45°N–49°N, 123°W–119°W) over 1920–2020 to those from June 25 to
104 July 4, 2021. Figure 1c shows JJA TXx averaged over all of the US stations in this re-
105 gion for each year. From Figures 1b,c, it is clear that the PNW heatwave was an out-
106 lier event compared to previous summertime maximum temperatures and will challenge
107 statistical modeling.

108 Philip et al. (2021) found that the 2021 spatially averaged temperatures from the
109 ERA5 reanalysis (Hersbach et al., 2020) exceeded the upper bound of an out of sample
110 non-stationary generalized extreme value (GEV) distribution fit to data from 1950 to
111 2020. They then included the 2021 values, estimating that the current return period of
112 the PNW heatwave was about 1000 years. Comparing this return period to that obtained
113 under preindustrial temperatures, they concluded that the probability of the PNW heat-
114 wave was increased by a factor of 390. Further analysis of climate model simulations and
115 their expert judgement caused them to conclude that the probability of the observed tem-
116 perature was increased by *at least* 150 as their final synthesis attribution statement.

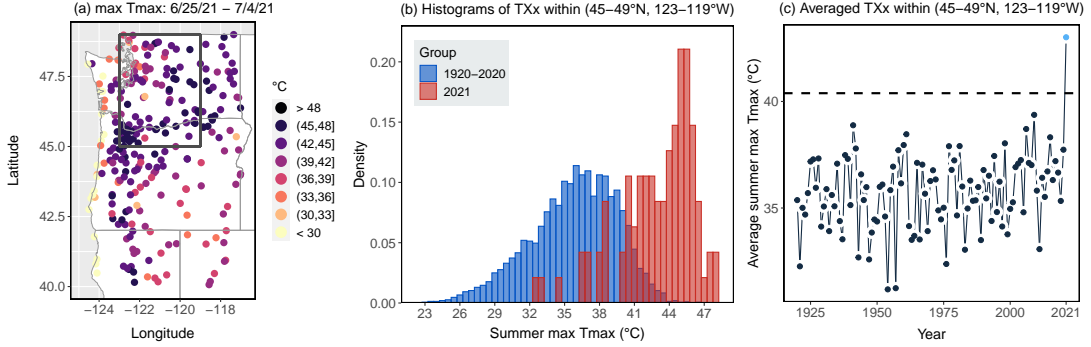


Figure 1. Observational station data from the Global Historical Climatology Network (GHCN) of (a) the maximum daily maximum temperature between June 25 and July 4, (b) histograms of the summertime (June/July/August, JJA) maximum daily maximum temperature (i.e., JJA TXx) from the US stations within the WWA region (45°N–49°N, 123°W–119°W), as defined by Philip et al. (2021), in 1920-2020 and in 2021 and (c) the average JJA TXx by year from the US stations within the same region. The dashed line is the Bayesian expectation of the upper bound on daily maximum temperature averaged across the US stations within the WWA region.

117 We repeat this non-stationary GEV analysis on individual station data from 1950-
 118 2020 instead of averaging over the WWA study region. In each single-station analysis,
 119 we use a GEV distribution with a location parameter linearly dependent on a sum-total
 120 forcing variable for five well-mixed greenhouse gases to accommodate non-stationarity
 121 (e.g. Risser et al. (2022)), which imposes a non-linear time trend in the GEV model. De-
 122 tails of the GEV analysis are discussed in Supplemental Section 1.

123 Figure 2a shows the Bayesian expectation of the upper bound for daily maximum
 124 temperatures for the 1950-2020 GHCN station data. Stations where the observed 2021
 125 values exceed the expectation of the upper bound (‘+’) reveal that most of the heatwave’s
 126 maximum temperatures are outside of the range of the GEV model. Figure 2b shows the
 127 2021 out of sample return times for the GHCN stations, where many stations realized
 128 return times in excess of 2000 years during the 2021 PNW heatwave. The probability
 129 of 2021 temperatures exceeding this GEV upper bound (Figure 2c) further illustrates
 130 that the out of sample GEV fails to describe the 2021 PNW heatwave. Including the 2021
 131 temperatures in the GEV fitting procedure extends the upper bounds to include these
 132 values in the distribution, but the distributions are a poor fit to the rest of the data. Us-
 133 ing a χ^2 goodness-of-fit test, the p -values calculated without 2021 values are generally
 134 greater than 0.2, demonstrating strong evidence of an underlying GEV distribution. How-
 135 ever, the p -values calculated when 2021 temperatures are included are less than 0.05, in-
 136 dicating that the distribution is significantly different from GEV. Figure 1b, constructed
 137 by binning all GHCN station data from 1920-2020 (blue) and 2021 (red), further sug-
 138 gests that the temperatures of the 2021 heatwave are drawn from different distributions
 139 than previous years that is not accounted for by the time-dependent greenhouse gas co-
 140 variate. The above evidence suggest that the critical GEV assumption of independent
 141 and identically distributed (i.i.d.) data is violated when 2021 temperatures are included.

142 Given that an in-sample GEV distribution is a poor fit to the GHCN data and that
 143 the combined effects of the atmospheric blocking pattern and anomalous AR were likely
 144 unique, we conclude that there should be little confidence in attribution statements based
 145 on in-sample GEV formulations. Philip et al. (2021) argued that the temperatures reached

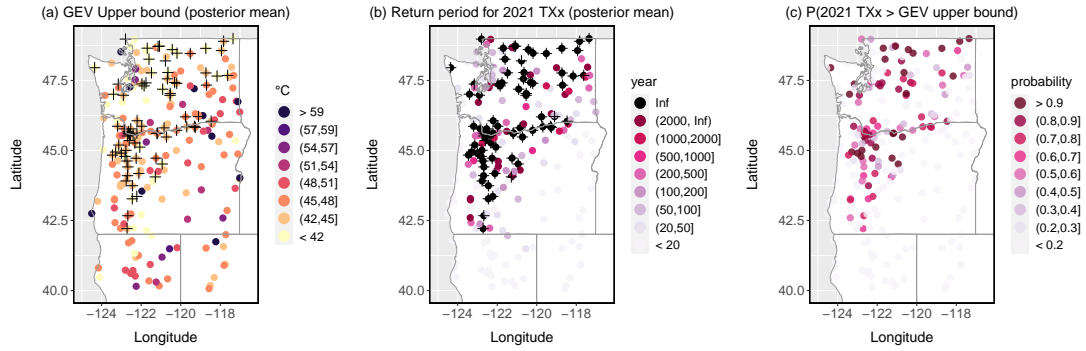


Figure 2. Results from fitting the non-stationary GEV distribution to station data from 1950 to 2020: (a) Bayesian expectation (posterior mean) for the GEV distributional upper bound; (b) Bayesian expectation for the return periods of 2021 JJA TXx (calculated using the fitted non-stationary GEV distribution). In both panels, ‘+’ signifies that the 2021 JJA TXx exceeded the Bayesian expectation of the GEV distributional upper bound, which leads to infinite return periods in (b); (c) The overall probability of 2021 TXx exceeding the GEV upper bound given the observations.

146 during the PNW heatwave were “virtually impossible” without climate change. How-
 147 ever, this is not supported from a purely Granger causal inference perspective (Ebert-
 148 Uphoff & Deng, 2012; Hannart et al., 2016) due to the failure of the GEV methodology.
 149 Our statistical analysis supports an attribution statement that these temperatures were
 150 virtually impossible under any previously experienced meteorological conditions, with
 151 or without global warming. Pearl causal inference statements (Pearl, 2009) about the
 152 change in magnitude of the PNW heatwave from global warming, assuming a fixed but
 153 unspecified return time, can be informed by climate models as discussed in the next sec-
 154 tion.

155 3 Dynamical Models and Experimental Design

156 From section 2, the PNW heatwave of 2021 was an extreme outlier event. Tradi-
 157 tionally, Pearl causal inference attribution statements are made with long simulations
 158 of global climate models, usually in pairs forced with both anthropogenic and natural
 159 forcing factors (Stott et al., 2016). However, another more conditional form of Pearl causal
 160 inference attribution statements can be formulated with the hindcast attribution (Wehner
 161 et al., 2019) or pseudo-global warming (PGW) method (Schär et al., 1996; Patricola &
 162 Wehner, 2018; Bercos-Hickey & Patricola, 2021; Bercos-Hickey et al., 2021; Patricola et
 163 al., 2022). In this approach, ensembles of regional climate model simulations are performed
 164 with historical initial and boundary conditions and are then compared with simulations
 165 performed with counterfactual initial and boundary conditions that have been adjusted
 166 by a climate change difference, or delta, that takes into account the thermodynamic com-
 167 ponent of anthropogenic climate change. While no attribution statement can be made
 168 about the human-induced change in probability of the event, quantitative attribution
 169 statements about the human-induced change in the magnitude of the event can be made
 170 with this more restricted approach.

171 In this study, the Weather Research and Forecasting (WRF) model (Skamarock
 172 et al., 2008) version 3.8.1 was used to perform hindcast simulations of the PNW heat-
 173 wave. To understand the impacts of model structural uncertainty, we performed a sim-
 174 ilar suite of simulations using the International Centre for Theoretical Physics Regional

175 Climate Model (RegCM) version 4.9.5 (Giorgi et al., 2012). The WRF hindcast simu-
 176 lations were initialized on June 24, 2021 0000 UTC and ran continuously through July
 177 4, 2021 with initial and boundary conditions from the 32 km resolution National Cen-
 178 ters for Environmental Prediction (NCEP) North American Regional Reanalysis (NARR).
 179 Further details of the WRF simulations are discussed in Supplemental Section 2. The
 180 RegCM hindcast simulations were initialized on June 22, 2021 0000 UTC and ran con-
 181 tinuously through July 02, 2021 with initial and boundary conditions from the Global
 182 Forecast System (GFS) version 4 0.5-degree analysis. Further details of the RegCM sim-
 183 ulations are discussed in Supplemental Section 3. Ten-member ensembles were performed
 184 for each model configuration and the effects of horizontal resolution were explored by
 185 configuring the models with grids of 18 km and 50 km spacings over the chosen domains
 186 (Figure S2).

187 To establish the validity of the heatwave simulations, we compare the WRF and
 188 RegCM hindcasts with observational and reanalysis data. As shown in Supplemental Sec-
 189 tion 4, the WRF and RegCM hindcasts accurately capture the key features of the PNW
 190 heatwave. The hindcasts of the heatwave event were best represented at 18 km (Sup-
 191 plemental Section 4), and thus for the remainder of the analysis we use the 18 km res-
 192 olution simulations.

193 In addition to the hindcast simulations, three ten-member ensembles under coun-
 194 terfactual conditions were performed using the PGW method to understand the effects
 195 of global warming on the PNW heatwave. The cooler “world that might have been” with-
 196 out the current amount of anthropogenic climate change permits attribution statements
 197 about the observed magnitude of the event. Two warmer “worlds that might be” sim-
 198 ulations were performed with mid- and late-21st century climate conditions under the
 199 Shared Socioeconomic Pathway 585 (SSP585) emissions scenario (O’Neill et al., 2016)
 200 to further elucidate the effect of global warming on the event. For the “world that might
 201 have been”, the deltas were calculated using the difference between historical and nat-
 202 urally forced (*hist-nat*) simulations from the multi-model average of the Coupled Model
 203 Intercomparison Project Phase 6 (CMIP6) (Danabasoglu, 2019) data (see Table S1). Thus
 204 the effects of anthropogenic forcing are removed but the natural solar and volcanic forc-
 205 ing effects are retained. The “world that might be” deltas were calculated using the dif-
 206 ference between the historical and mid- and late-21st century future SSP585 simulations
 207 from the CMIP6 multi-model average. Additional details on the PGW experiments are
 208 discussed in Supplemental Section 5. Lastly, to examine the effects of climate change on
 209 soil moisture-temperature feedbacks, *hist-nat*, mid-, and late-21st century experiments
 210 were conducted with the 18 km WRF model by additionally altering soil moisture. A
 211 summary of all model experiments is shown in Table S2.

212 In the following section, our analyses utilize spatial averages over the region 45°N-
 213 52°N and 124°W-119°W (Figure S2). Because WRF and RegCM were run at finer res-
 214 olution than the CMIP-class models in Philip et al. (2021), we extended the region of
 215 interest to the west to be closer to the coast than the WWA region.

216 4 Changes in PNW heatwave temperature

217 The effects of the current amount of climate change on the PNW heatwave are as-
 218 sessed by comparing the WRF and RegCM simulations in the historical and *hist-nat* cli-
 219 mates. Figure 3 shows the June 25-July 1, 2021 time series of (a) the GHCN, NARR,
 220 GFS, WRF, and RegCM daily maximum temperature and (b) the WRF and RegCM
 221 temperature differences between the climate scenarios and the historical. Contours of
 222 the maximum temperature on June 28, the hottest day of the GHCN station observa-
 223 tions (Figure 3a), are shown for the (c)(f) historical, (d)(g) historical minus *hist-nat*, and
 224 (e)(h) late-century minus historical simulations from the 18 km (c)-(e) WRF and (f)-
 225 (h) RegCM. From Figure 3d, the WRF model clearly exhibits warming from the *hist-*

226 nat to the historical climate except for some cooling at the Oregon coast. From Figure
 227 3g, the RegCM model exhibits a more heterogeneous warming and the cooling is shifted
 228 northward to the coast of British Columbia. In our analysis region (Figures 3c,f black
 229 box), the ensemble average increase in the daily maximum two-meter temperature on
 230 June 28 is $0.95\pm 0.22^\circ\text{C}$ for WRF and $0.66\pm 0.05^\circ\text{C}$ for RegCM from the hist-nat to the
 231 historical, where the uncertainty bounds are calculated from the standard error. Over
 232 the four-day period June 27-30, during which multiple temperature records were broken,
 233 the average increase in daily maximum two-meter temperature is $0.98\pm 0.40^\circ\text{C}$ for
 234 WRF and $0.78\pm 0.07^\circ\text{C}$ for RegCM from the hist-nat to the historical. The blue lines
 235 in Figure 3b reveal that the attributable warming in the WRF model averaged over the
 236 region of interest (about 1°C) does not change much during the heatwave event. The RegCM,
 237 which here differs from the WRF model in that soil moisture was not altered in the hist-
 238 nat simulations, exhibits a decrease in attributable warming until June 28 and then an
 239 increase until July 1.

240 Figure 3e shows that the WRF simulated heatwave is warmer over the entire domain
 241 under late-century conditions when compared to the historical simulations. Similar
 242 warming is also seen in the WRF simulations under mid-century conditions (not shown).
 243 In contrast, Figure 3h shows that while the RegCM model warms over the majority of
 244 the region under late-century conditions, cooling is simulated along the coast of southern
 245 Oregon and northern California. This coastal cooling in the RegCM late-century sim-
 246 ulations is likely due to a complicated interaction between changes in onshore winds and
 247 a warmed ocean and is influenced by the choice of boundary layer parameterization scheme.
 248 In our analysis region (Figures 3c,f black box), the average increase in the daily maximum
 249 two-meter temperature on June 28 is $1.55\pm 0.29^\circ\text{C}$ for WRF from the historical
 250 to the mid-century, and is $4.68\pm 0.26^\circ\text{C}$ for WRF and $4.57\pm 0.04^\circ\text{C}$ for RegCM from the
 251 historical to the late-century. During the peak days of the heatwave, the June 27-30 average
 252 increase in maximum daily two-meter temperature is $1.71\pm 0.39^\circ\text{C}$ for WRF from
 253 the historical to the mid-century, and is $5.41\pm 0.41^\circ\text{C}$ for WRF and $5.20\pm 0.06^\circ\text{C}$ for RegCM
 254 from the historical to the late-century.

255 The red lines in Figure 3b compare the regionally averaged temperature change between
 256 the present and late-century under SSP585 forcing conditions. The orange line shows
 257 a similar result for the WRF model under mid-century SSP585 forcing conditions. In
 258 these warmer simulations, the anthropogenic warming of the PNW heatwave gradually
 259 reduces until the hottest days are reached, June 29, 2021. Afterwards, the anthropogenic
 260 warming increases as the heatwave evolves for both models, lengthening the duration of
 261 the heatwave in both the WRF and RegCM simulations. This behavior is also exhibited
 262 in the RegCM historical compared to hist-nat simulations (blue dashed line), but
 263 is not for WRF, where the regionally averaged anthropogenic warming is relatively constant
 264 over the entire duration of the simulation.

265 To examine the effects of soil moisture-temperature feedback on the PNW heat-
 266 wave, we performed WRF experiments with and without the soil moisture delta. Inclu-
 267 sion of the soil moisture delta causes warmer climates to have drier soil and cooler cli-
 268 mates to have wetter soil. Figure 4 shows the June 28, 2021 ensemble-averaged maxi-
 269 mum two-meter temperature from the 18 km WRF (a) hist-nat, (b) mid-century, and
 270 (c) late-century experiments with the soil moisture delta minus the experiments with-
 271 out the soil moisture delta. Panel (d) shows the June 25-July 1 time series of the daily
 272 maximum temperature in the soil moisture minus no soil moisture experiments. From
 273 Figure 4a, the heatwave in the hist-nat climate is cooler across most of the region when
 274 the soil moisture delta is included, reflecting an increase in evapotranspiration cooling.
 275 In our analysis region (Figures 3c,f black box), the average daily maximum two-meter
 276 temperature in Figure 4a is $0.10\pm 0.21^\circ\text{C}$ cooler in the hist-nat experiment with the soil
 277 moisture delta than it is without. Figures 4b,c indicate that the heatwave in the mid-
 278 and late-century climates is warmer across almost all of the region when the soil mois-

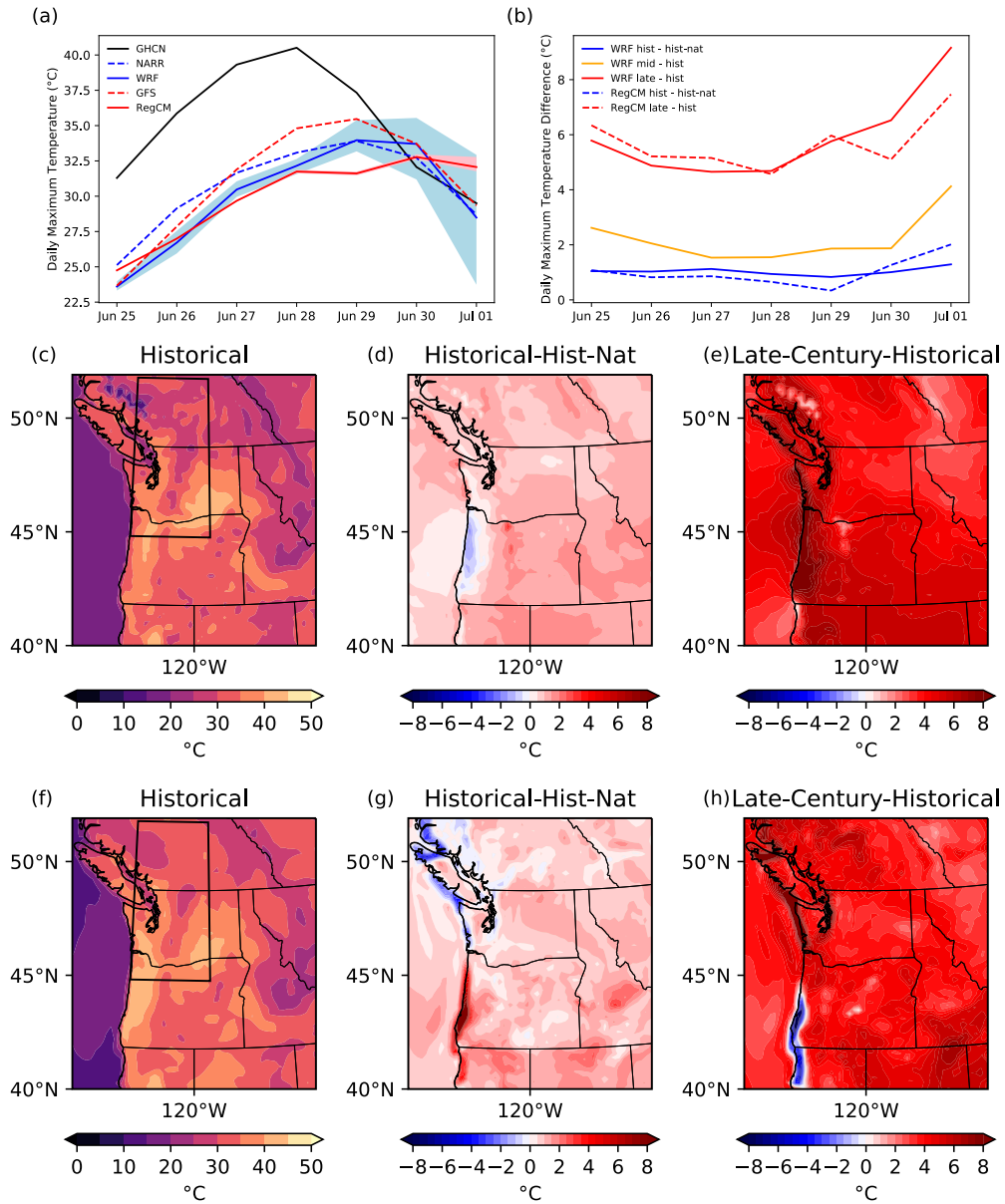


Figure 3. June 25–July 1, 2021 daily maximum temperature (a) from the GHCN, NARR, GFS, and the WRF and RegCM historical 18 km ensembles, and daily maximum temperature difference (b) between the WRF and RegCM historical and hist-nat, mid-century (WRF only), and late-century ensembles averaged over the region 45°N–52°N and 124°W–119°W. The shading in panel (a) shows the range of values over the WRF and RegCM 10-member ensembles. Ensemble-averaged daily maximum 2 m temperature (°C) on June 28 of the (c)(f) historical, (d)(g) historical minus hist-nat, and (e)(h) late-century minus historical simulations from the 18 km (c)–(e) WRF with the soil moisture delta and (f)–(h) RegCM. Black boxes in panels (c) and (f) are the regions used for spatial averaging, also shown in Figure S2.

279 ture delta is included, reflecting a decrease in evapotranspiration cooling due to less avail-
 280 able soil moisture. The average daily maximum two-meter temperature in Figures 4b,c
 281 is $0.78\pm 0.34^{\circ}\text{C}$ and $0.90\pm 0.28^{\circ}\text{C}$ warmer in the mid- and late-century experiments with
 282 the soil moisture delta, respectively.

283 The blue line in Figure 4d reveals that the effects of soil moisture on the hist-nat
 284 simulations remains relatively constant throughout the duration of the heatwave. In con-
 285 trast, the future climate simulations (Figure 4d orange and red lines) exhibit a tempo-
 286 rally dependent enhancement of the effects of the soil moisture delta as the heatwave pro-
 287 gresses. Roughly following the simulated temperature itself (Figure 3a), the effect of de-
 288 creased soil moisture peaks at about 1.0°C and 1.2°C warmer in the mid- and late-century
 289 experiments, respectively.

290 5 Conclusions

291 The 2021 Pacific Northwest (PNW) heatwave was a rare and unprecedented com-
 292 pound weather event. An unusual summertime atmospheric river interacted with an omega
 293 block pattern and preexisting dry soil conditions to shatter century-old temperature records
 294 by several degrees Centigrade. While there is little doubt that anthropogenic global warm-
 295 ing contributed to the probability and magnitude of the extreme temperatures, the unique-
 296 ness of the event precludes quantifying this influence by traditional event attribution meth-
 297 ods. In section 2, we demonstrated that out of sample fitted non-stationary Generalized
 298 Extreme Value (GEV) distributions fail to contain many of the observed 2021 observa-
 299 tions within the uncertainty estimates of their upper bounds. While including the 2021
 300 temperatures in the GEV fitting procedure extends the upper bounds to include these
 301 values in the distribution, these distributions are a poor fit to the rest of the data. The
 302 underlying reason for this failure of traditional statistical methods is that the unique-
 303 ness of the 2021 PNW heatwave violates the i.i.d. assumption of GEV theory. We there-
 304 fore conclude that estimates of the PNW heatwave return times are not accurate and
 305 that confidence in GEV-based estimates of the human influence on the change in the prob-
 306 ability of the observed extreme temperatures should be low. We further conclude that
 307 quantitative changes in event magnitude and frequency from CMIP-class models (Wehner
 308 et al., 2020, 2018; Philip et al., 2021) are made with low confidence as it is not clear that
 309 global climate models can adequately simulate the relevant meteorological phenomena
 310 of the PNW heatwave (van Oldenborgh et al., 2021, 2022).

311 In sections 3,4, we present an alternative but more limited attribution of the an-
 312 thropogenic changes to the PNW heatwave using ensembles of simulations from the re-
 313 gional models WRF and RegCM, where the pseudo-global warming (PGW) method was
 314 used to examine the effects of removing anthropogenic warming and additional future
 315 warming. We find that the historical model simulations are in agreement with their ini-
 316 tial and boundary condition datasets, but that the observed and simulated gridded prod-
 317 ucts are cooler than station observations during the hot portion of the event. Compar-
 318 ison of the historical heatwave with a counterfactual heatwave in a world without human-
 319 induced warming indicates that the anthropogenic temperature increase is about 1°C
 320 and relatively constant over the course of the event. In contrast, the heatwave in an SSP585
 321 world with significant future warming would be 5°C warmer, and the anthropogenic in-
 322 fluence extends the peak of the heatwave, indicating a future increase in heatwave du-
 323 ration.

324 These anthropogenic increases in extreme temperatures during the PNW heatwave
 325 are less than previous estimates (Philip et al., 2021). One possible reason for this is that
 326 severe drought conditions were being experienced in June 2021 in much of the southern
 327 portion of our analysis region, reducing the evapotranspiration cooling in our cooler coun-
 328 terfactual “world that might have been”. In section 4, we examined the effects of soil
 329 moisture in the PGW experiments and found that, at current levels of global warming,

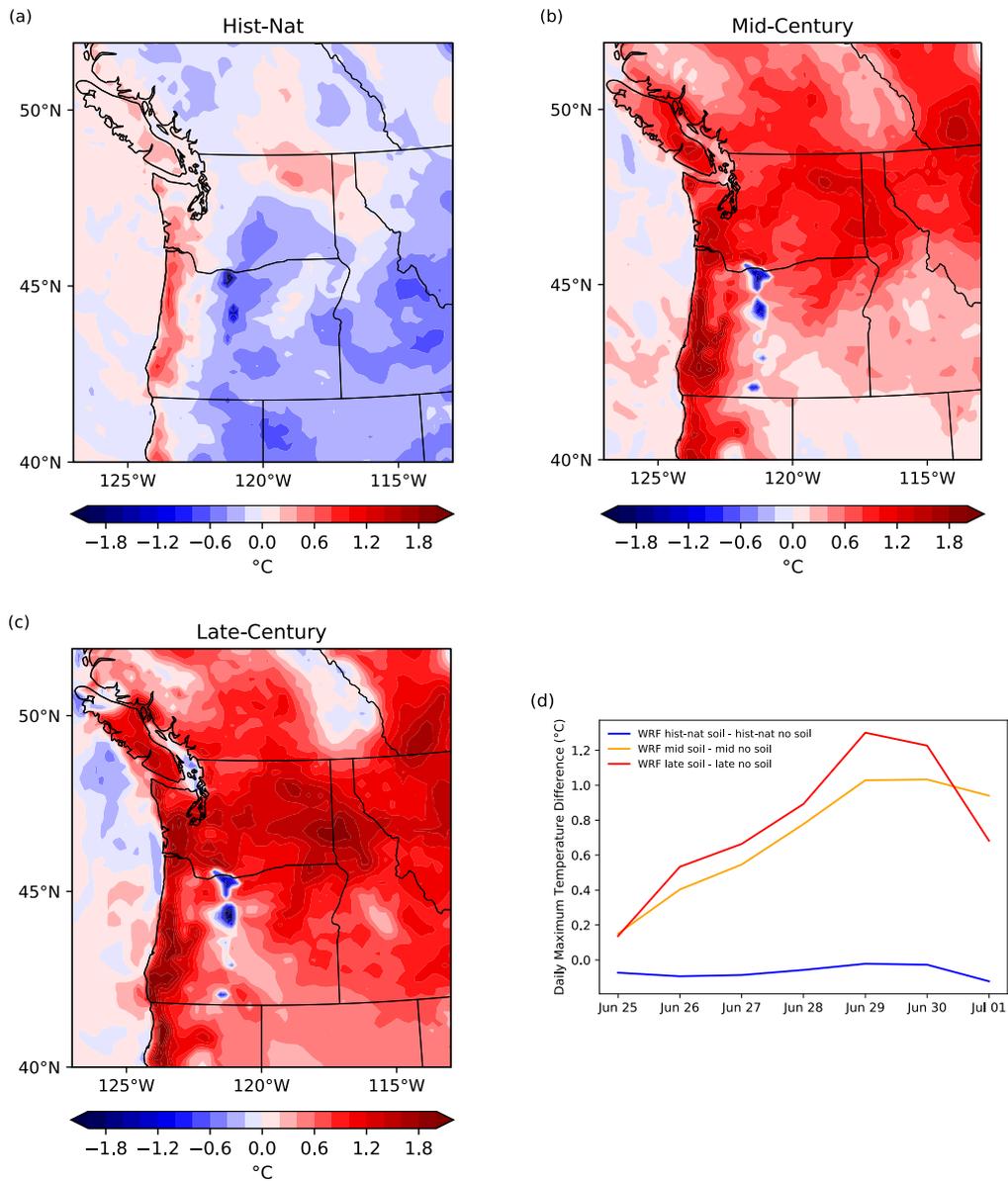


Figure 4. Ensemble-averaged daily maximum 2 m temperature ($^{\circ}\text{C}$) on June 28, 2021 from the 18 km WRF (a) hist-nat, (b) mid-century, and (c) late-century experiments with the soil moisture delta minus the experiments without the soil moisture delta. The June 25-July 1, 2021 daily maximum temperature difference between the experiments with and without the soil moisture delta averaged over the region 45°N - 52°N and 124°W - 119°W (d).

330 this cooling is altered by only about 0.10°C. As precursor soil conditions from the drought
 331 are drier than the average conditions used in traditional CMIP-class heatwave attribu-
 332 tion statements, this is not unexpected. Even in much warmer late-century conditions,
 333 the maximum soil moisture-temperature feedback is 1.2°C out of over 6°C averaged over
 334 our analysis region. While it may be that the amplification of the anthropogenic tem-
 335 perature change during heatwaves (Seneviratne et al., 2021) is diminished by pre-existing
 336 drought conditions, this is not the case in much warmer future simulations. Clearly, our
 337 understanding of all the physical mechanisms behind this extreme heatwave and their
 338 anthropogenic changes is limited (van Oldenborgh et al., 2022) and our traditional at-
 339 tribution tools fail for this and other extreme outlier events. However, there may be op-
 340 portunities to remedy this by examining the large coupled and uncoupled model ensem-
 341 bles (Kay et al., 2015; Stone et al., 2019). Presently, however, we do not know with con-
 342 fidence whether the 2021 PNW heatwave and the associated weather patterns will re-
 343 main an outlier event or is a harbinger of things to come.

344 Open Research

345 The WRF and RegCM simulation data used for the pseudo-global warming anal-
 346 ysis in the study are available at https://portal.neresc.gov/cascade/PNW_Heatwave. CMIP6
 347 data is available through Danabasoglu (2019).

348 Acknowledgments

349 This material is based upon work supported by the U.S. Department of Energy, Office
 350 of Science, Office of Biological and Environmental Research, Climate and Environmen-
 351 tal Sciences Division, Regional & Global Model Analysis Program, under Award Num-
 352 ber DE-AC02-05CH11231. This research used resources of the National Energy Research
 353 Scientific Computing Center (NERSC), a DOE Office of Science User Facility supported
 354 by the Office of Science of the U.S. DOE under Contract No. DE-AC02-05CH11231. We
 355 acknowledge the World Climate Research Programme, which, through its Working Group
 356 on Coupled Modelling, coordinated and promoted CMIP6. We thank the climate mod-
 357 eling groups for producing and making available their model output, the Earth System
 358 Grid Federation (ESGF) for archiving the data and providing access, and the multiple
 359 funding agencies who support CMIP6 and ESGF. This project was also partially sup-
 360 ported by the Environmental Resilience Institute, funded by Indiana University’s Pre-
 361 pared for Environmental Change Grand Challenge initiative.

362 References

- 363 Baker, M., & Sergio, O. (2021). The pacific northwest, built for mild summers, is
 364 scorching yet again. *New York Times*.
- 365 Bercos-Hickey, E., & Patricola, C. M. (2021). Anthropogenic influences on the
 366 african easterly jet–african easterly wave system. *Climate Dynamics*. doi:
 367 10.1007/s00382-021-05838-1
- 368 Bercos-Hickey, E., Patricola, C. M., & Gallus, W. A. (2021). Anthropogenic In-
 369 fluences on Tornadic Storms. *Journal of Climate*, *34*(22), 8989–9006. Re-
 370 trieved from [https://journals.ametsoc.org/view/journals/clim/aop/](https://journals.ametsoc.org/view/journals/clim/aop/JCLI-D-20-0901.1/JCLI-D-20-0901.1.xml)
 371 [JCLI-D-20-0901.1/JCLI-D-20-0901.1.xml](https://journals.ametsoc.org/view/journals/clim/aop/JCLI-D-20-0901.1/JCLI-D-20-0901.1.xml) doi: 10.1175/JCLI-D-20-0901.1
- 372 Berner, J., Ha, S.-Y., Hacker, J. P., Fournier, A., & Snyder, C. (2011). Model
 373 uncertainty in a mesoscale ensemble prediction system: Stochastic versus mul-
 374 tiphysics representations. *Monthly Weather Review*, *139*(6), 1972-1995.
- 375 Black, E., Blackburn, M., Harrison, G., Hoskins, B., & Methven, J. (2004). Factors
 376 contributing to the summer 2003 european heatwave. *Weather*, *59*(8), 217-223.
 377 doi: <https://doi.org/10.1256/wea.74.04>
- 378 Campbell, S., Remenyi, T. A., White, C. J., & Johnston, F. H. (2018). Heatwave

- 379 and health impact research: A global review. *Health & Place*, *53*, 210-218.
- 380 Chen, F., & Dudhia, J. (2001). Coupling an advanced land surface–hydrology model
381 with the penn state–ncar mm5 modeling system. part i: Model implementation
382 and sensitivity. *Monthly Weather Review*, *129*(4), 569-585.
- 383 Danabasoglu, G. (2019). *NCAR CESM2 model output prepared for CMIP6 CMIP*.
384 Earth System Grid Federation. Retrieved from [https://doi.org/10.22033/](https://doi.org/10.22033/ESGF/CMIP6.2185)
385 [ESGF/CMIP6.2185](https://doi.org/10.22033/ESGF/CMIP6.2185) doi: 10.22033/ESGF/CMIP6.2185
- 386 Dickinson, R. E., Henderson-Sellers, A., Kennedy, P. J., & Wilson, M. F. (1993).
387 Biosphere atmosphere transfer scheme (BATS) version 1e as coupled for Com-
388 munity Climate Model. *NCAR Tech. Note NCAR/TN-378+SR*(August), 77.
389 doi: 10.1029/2009JD012049
- 390 Diffenbaugh, N. S., & Ashfaq, M. (2010). Intensification of hot extremes in the
391 united states. *Geophysical Research Letters*, *37*(15). doi: [https://doi.org/10](https://doi.org/10.1029/2010GL043888)
392 [.1029/2010GL043888](https://doi.org/10.1029/2010GL043888)
- 393 Di Liberto, T. (2021). Astounding heat obliterates all-time records across the
394 pacific northwest and western canada in june 2021. *National Oceanic and*
395 *Atmospheric Administration*. Retrieved from [https://www.climate.gov/](https://www.climate.gov/news-features/event-tracker/astounding-heat-obliterates-all-time-records-across-pacific-northwest)
396 [news-features/event-tracker/astounding-heat-obliterates-all-time](https://www.climate.gov/news-features/event-tracker/astounding-heat-obliterates-all-time-records-across-pacific-northwest)
397 [-records-across-pacific-northwest](https://www.climate.gov/news-features/event-tracker/astounding-heat-obliterates-all-time-records-across-pacific-northwest)
- 398 Dole, R., Hoerling, M., Perlwitz, J., Eischeid, J., Pegion, P., Zhang, T., ... Murray,
399 D. (2011). Was there a basis for anticipating the 2010 russian heat wave? *Geo-*
400 *physical Research Letters*, *38*(6). doi: <https://doi.org/10.1029/2010GL046582>
- 401 Ebert-Uphoff, I., & Deng, Y. (2012). Causal discovery for climate research
402 using graphical models. *Journal of Climate*, *25*(17), 5648 - 5665. Re-
403 trieved from [https://journals.ametsoc.org/view/journals/clim/25/](https://journals.ametsoc.org/view/journals/clim/25/17/jcli-d-11-00387.1.xml)
404 [17/jcli-d-11-00387.1.xml](https://journals.ametsoc.org/view/journals/clim/25/17/jcli-d-11-00387.1.xml) doi: 10.1175/JCLI-D-11-00387.1
- 405 Emanuel, K. A. (1991, nov). A Scheme for Representing Cumulus Con-
406 vection in Large-Scale Models. *Journal of the Atmospheric Sciences*,
407 *48*(21), 2313–2329. Retrieved from [http://journals.ametsoc.org/](http://journals.ametsoc.org/doi/10.1175/1520-0469(1991)048%3C2313:ASFRCC%3E2.0.CO;2)
408 [doi/10.1175/1520-0469\(1991\)048%3C2313:ASFRCC%3E2.0.CO;2](http://journals.ametsoc.org/doi/10.1175/1520-0469(1991)048%3C2313:ASFRCC%3E2.0.CO;2) doi:
409 [10.1175/1520-0469\(1991\)048%3C2313:ASFRCC%3E2.0.CO;2](http://journals.ametsoc.org/doi/10.1175/1520-0469(1991)048%3C2313:ASFRCC%3E2.0.CO;2)
- 410 Emanuel, K. A., & Živković-Rothman, M. (1999, jun). Development and Eval-
411 uation of a Convection Scheme for Use in Climate Models. *Journal of*
412 *the Atmospheric Sciences*, *56*(11), 1766–1782. Retrieved from [http://](http://journals.ametsoc.org/doi/10.1175/1520-0469(1999)056%3C1766:DAEOAC%3E2.0.CO;2)
413 [journals.ametsoc.org/doi/10.1175/1520-0469\(1999\)056%3C1766:DAEOAC%](http://journals.ametsoc.org/doi/10.1175/1520-0469(1999)056%3C1766:DAEOAC%3E2.0.CO;2)
414 [3E2.0.CO;2](http://journals.ametsoc.org/doi/10.1175/1520-0469(1999)056%3C1766:DAEOAC%3E2.0.CO;2) doi: 10.1175/1520-0469(1999)056%3C1766:DAEOAC%3E2.0.CO;2
- 415 Etminan, M., Myhre, G., Highwood, E., & Shine, K. (2016). Radiative forcing
416 of carbon dioxide, methane, and nitrous oxide: A significant revision of the
417 methane radiative forcing. *Geophysical Research Letters*, *43*(24), 12–614.
- 418 Eyring, V., Bony, S., Meehl, G. A., Senior, C. A., Stevens, B., Stouffer, R. J., &
419 Taylor, K. E. (2016). Overview of the coupled model intercomparison project
420 phase 6 (cmip6) experimental design and organization. *Geosci. Model Dev.*,
421 *9*(5), 1937-1958. doi: 10.5194/gmd-9-1937-2016
- 422 Giorgi, F., Coppola, E., Solmon, F., Mariotti, L., Sylla, M., Bi, X., ... Brankovic,
423 C. (2012). RegCM4: model description and preliminary tests over mul-
424 tiple CORDEX domains. *Climate Research*, *52*, 7–29. Retrieved from
425 <http://www.int-res.com/abstracts/cr/v52/p7-29/> doi: 10.3354/cr01018
- 426 Grell, G. A., & Freitas, S. R. (2014). A scale and aerosol aware stochastic convective
427 parameterization for weather and air quality modeling. *Atmos. Chem. Phys.*,
428 *14*(10), 5233-5250.
- 429 Grenier, H., & Bretherton, C. S. (2001). A Moist PBL Parameterization for Large-
430 Scale Models and Its Application to Subtropical Cloud-Topped Marine Bound-
431 ary Layers. *Monthly Weather Review*, *129*(3), 357–377. Retrieved from
432 [http://dx.doi.org/10.1175/1520-0493\(2001\)129%3C0357:AMPPFL%3E2.0](http://dx.doi.org/10.1175/1520-0493(2001)129%3C0357:AMPPFL%3E2.0.CO;5Cn2)
433 [.CO;5Cn2](http://dx.doi.org/10.1175/1520-0493(2001)129%3C0357:AMPPFL%3E2.0.CO;5Cn2) doi: 10.1175/1520-0493(2001)129%3C0357:AMPPFL%3E2.0.CO;2

- 434 Hannart, A., Pearl, J., Otto, F. E. L., Naveau, P., & Ghil, M. (2016, jan).
 435 Causal Counterfactual Theory for the Attribution of Weather and Climate-
 436 Related Events. *Bulletin of the American Meteorological Society*, *97*(1),
 437 99–110. Retrieved from [http://journals.ametsoc.org/doi/abs/10.1175/](http://journals.ametsoc.org/doi/abs/10.1175/BAMS-D-14-00034.1)
 438 [BAMS-D-14-00034.1](http://journals.ametsoc.org/doi/abs/10.1175/BAMS-D-14-00034.1) doi: 10.1175/BAMS-D-14-00034.1
- 439 Hersbach, H., Bell, B., Berrisford, P., Hirahara, S., Horányi, A., Muñoz-Sabater, J.,
 440 ... others (2020). The era5 global reanalysis. *Quarterly Journal of the Royal*
 441 *Meteorological Society*, *146*(730), 1999–2049.
- 442 Hodnebrog, Ø., Etminan, M., Fuglestedt, J., Marston, G., Myhre, G., Nielsen, C.,
 443 ... Wallington, T. (2013). Global warming potentials and radiative efficiencies
 444 of halocarbons and related compounds: A comprehensive review. *Reviews of*
 445 *Geophysics*, *51*(2), 300–378.
- 446 Hong, S.-Y., & Lim, J.-O. J. (2006). The wrf single-moment 6-class microphysics
 447 scheme (wsm6). *Journal of the Korean Meteorological Society*, *42*(2), 129-151.
- 448 Hong, S.-Y., & Pan, H.-L. (1996). Nonlocal boundary layer vertical diffusion in a
 449 medium-range forecast model. *Monthly Weather Review*, *124*(10), 2322-2339.
- 450 Horton, D. E., Johnson, N. C., Singh, D., Swain, D. L., Rajaratnam, B., & Diff-
 451 enbaugh, N. S. (2015). Contribution of changes in atmospheric circulation
 452 patterns to extreme temperature trends. *Nature*, *522*(7557), 465-469.
- 453 Iacono, M. J., Delamere, J. S., Mlawer, E. J., Shephard, M. W., Clough, S. A., &
 454 Collins, W. D. (2008). Radiative forcing by long-lived greenhouse gases:
 455 Calculations with the aer radiative transfer models. *Journal of Geophysical*
 456 *Research*, *113*(D13), D13103.
- 457 Kay, J. E., Deser, C., Phillips, A., Mai, A., Hannay, C., Strand, G., ... Vertenstein,
 458 M. (2015). The Community Earth System Model (CESM) Large Ensemble
 459 Project: A Community Resource for Studying Climate Change in the Pres-
 460 ence of Internal Climate Variability. *Bulletin of the American Meteorological*
 461 *Society*, *96*(8), 1333–1349. doi: 10.1175/BAMS-D-13-00255.1
- 462 Kiehl, J., Hack, J., Bonan, G., Boville, B., Briegleb, B., Williamson, D., & Rasch, P.
 463 (1996). *Description of the NCAR Community Climate Model (CCM3)* (Tech.
 464 Rep. No. September). doi: 10.5065/D6FF3Q99
- 465 Lin, H., Mo, R., & Vitart, F. (2022). The 2021 western north american heatwave
 466 and its subseasonal predictions. *Geophysical Research Letters*, e2021GL097036.
 467 doi: <https://doi.org/10.1029/2021GL097036>
- 468 McEvoy, D., Ahmed, I., & Mullett, J. (2009). The impact of the 2009 heat wave on
 469 melbourne’s critical infrastructure. *Local Environment*, *17*(8), 783-796.
- 470 Meehl, G. A., & Tebaldi, C. (2004). More intense, more frequent, and longer lasting
 471 heat waves in the 21st century. *Science*, *305*(5686), 994 LP - 997.
- 472 Meinshausen, M., & Nicholls, Z. R. J. (2018). *Uom-remind-maggie-ssp585-1-2-*
 473 *0: Remind-maggie-ssp585 ghg concentrations*. Earth System Grid Federation.
 474 Retrieved from <https://doi.org/10.22033/ESGF/input4MIPs.2349> doi: 10
 475 .22033/ESGF/input4MIPs.2349
- 476 Meinshausen, M., & Vogel, E. (2016). *input4mips.uom.ghgconcentrations.cmip.uom-*
 477 *cmip-1-2-0*. Earth System Grid Federation. doi: 10.22033/ESGF/input4MIPs
 478 .1118
- 479 Min, S.-K., Zhang, X., Zwiers, F., Shiogama, H., Tung, Y.-S., & Wehner, M. (2013,
 480 jun). Multimodel Detection and Attribution of Extreme Temperature Changes.
 481 *Journal of Climate*, *26*(19), 7430–7451. doi: 10.1175/JCLI-D-12-00551.1
- 482 Miralles, D. G., Teuling, A. J., van Heerwaarden, C. C., & Vilà-Guerau de Arel-
 483 lano, J. (2014, may). Mega-heatwave temperatures due to combined soil
 484 desiccation and atmospheric heat accumulation. *Nature Geoscience*, *7*(5),
 485 345–349. Retrieved from <http://www.nature.com/articles/ngeo2141> doi:
 486 10.1038/ngeo2141
- 487 Mo, R., Lin, H., & Vitart, F. (2022). An anomalous atmospheric river linked to the
 488 late june 2021 western north america heatwave. *Commun. Earth Environ..* (in

- 489 revision)
- 490 Neal, E., Huang, C. S. Y., & Nakamura, N. (2022). The 2021 pacific north-
 491 west heat wave and associated blocking: Meteorology and the role of
 492 an upstream cyclone as a diabatic source of wave activity. *Geophysi-
 493 cal Research Letters*, *49*(8), e2021GL097699. Retrieved from [https://
 494 agupubs.onlinelibrary.wiley.com/doi/abs/10.1029/2021GL097699](https://agupubs.onlinelibrary.wiley.com/doi/abs/10.1029/2021GL097699)
 495 (e2021GL097699 2021GL097699) doi: <https://doi.org/10.1029/2021GL097699>
- 496 O'Brien, T. A., Chuang, P. Y., Sloan, L. C., Faloon, I. C., & Rossiter, D. L. (2012).
 497 Coupling a new turbulence parametrization to RegCM adds realistic stra-
 498 tocumulus clouds. *Geoscientific Model Development*, *5*(4), 989–1008. doi:
 499 10.5194/gmd-5-989-2012
- 500 O'Brien, T. A., Sloan, L. C., & Snyder, M. A. (2011, sep). Can ensembles of re-
 501 gional climate model simulations improve results from sensitivity studies? *Cli-
 502 mate Dynamics*, *37*(5-6), 1111–1118. Retrieved from [http://link.springer
 503 .com/10.1007/s00382-010-0900-5](http://link.springer.com/10.1007/s00382-010-0900-5) doi: 10.1007/s00382-010-0900-5
- 504 O'Neill, B. C., Tebaldi, C., Van Vuuren, D. P., Eyring, V., Friedlingstein, P., Hurtt,
 505 G., ... Sanderson, B. M. (2016). The Scenario Model Intercomparison Project
 506 (ScenarioMIP) for CMIP6. *Geoscientific Model Development*, *9*(9), 3461–3482.
 507 doi: 10.5194/gmd-9-3461-2016
- 508 Patricola, C. M., & Wehner, M. F. (2018). Anthropogenic influences on major tropi-
 509 cal cyclone events. *Nature*, *563*(7731), 339–346.
- 510 Patricola, C. M., Wehner, M. F., Bercos-Hickey, E., Maciel, F. V., May, C., Mak,
 511 M., ... Leal, S. (2022). Future changes in extreme precipitation over the san
 512 francisco bay area: Dependence on atmospheric river and extratropical cyclone
 513 events. *Weather and Climate Extremes*, *36*, 100440. Retrieved from [https://
 514 www.sciencedirect.com/science/article/pii/S2212094722000275](https://www.sciencedirect.com/science/article/pii/S2212094722000275) doi:
 515 <https://doi.org/10.1016/j.wace.2022.100440>
- 516 Pearl, J. (2009). *Causality*. Cambridge, U. K., Cambridge University Press.
- 517 Perkins, S. E. (2015). A review on the scientific understanding of heatwaves—their
 518 measurement, driving mechanisms, and changes at the global scale. *Atmo-
 519 spheric Research*, *164-165*, 242–267.
- 520 Perkins, S. E., Alexander, L. V., & Nairn, J. R. (2012). Increasing frequency, in-
 521 tensity and duration of observed global heatwaves and warm spells. *Geophysi-
 522 cal Research Letters*, *39*(20). doi: <https://doi.org/10.1029/2012GL053361>
- 523 Perkins-Kirkpatrick, S. E., & Alexander, L. V. (2013). On the measurement of heat
 524 waves. *Journal of Climate*, *26*(13), 4500–4517.
- 525 Perkins-Kirkpatrick, S. E., & Gibson, P. B. (2017). Changes in regional heatwave
 526 characteristics as a function of increasing global temperature. *Scientific Re-
 527 ports*, *7*(1), 12256.
- 528 Philip, S. Y., Kew, S. F., van Oldenborgh, G. J., Anslow, F. S., Seneviratne,
 529 S. I., Vautard, R., ... Otto, F. E. L. (2021). Rapid attribution analy-
 530 sis of the extraordinary heatwave on the pacific coast of the us and canada
 531 june 2021. *Earth System Dynamics Discussions*, *2021*, 1–34. Retrieved
 532 from [https://esd.copernicus.org/preprints/esd-2021-90/
 533 10.5194/esd-2021-90](https://esd.copernicus.org/preprints/esd-2021-90/) doi:
 10.5194/esd-2021-90
- 534 Popovich, N., & Choi-Schagrin, W. (2021). Hidden toll of the northwest heat wave:
 535 Hundreds of extra deaths. *New York Times*.
- 536 Rex, D. F. (1950). Blocking action in the middle troposphere and its effect upon re-
 537 gional climate. *Tellus*, *2*(4), 275–301.
- 538 Risser, M., Collins, W., Wehner, M., O'Brien, T., Paciorek, C., O'Brien, J., ...
 539 Loring, B. (2022). A framework for detection and attribution of regional pre-
 540 cipitation change: Application to the United States historical record. *Climate
 541 Dynamics*. doi: <https://doi.org/10.21203/rs.3.rs-785460/v1>
- 542 Risser, M., Wehner, M., O'Brien, J., Patricola, C., O'Brien, T., Collins, W., ...
 543 Huang, H. (2021). Quantifying the influence of natural climate variability

- 544 on in situ measurements of seasonal total and extreme daily precipitation.
 545 *Climate Dynamics*. doi: 10.1007/s00382-021-05638-7
- 546 Ruffault, J., Curt, T., Moron, V., Trigo, R. M., Mouillot, F., Koutsias, N., ...
 547 Belhadj-Khedher, C. (2020). Increased likelihood of heat-induced large wild-
 548 fires in the mediterranean basin. *Scientific Reports*, 10(1), 13790.
- 549 Schaller, N., Sillmann, J., Anstey, J., Fischer, E. M., Grams, C. M., & Russo, S.
 550 (2018). Influence of blocking on northern european and western russian heat-
 551 waves in large climate model ensembles. *Environmental Research Letters*,
 552 13(5).
- 553 Schär, C., Frei, C., Lüthi, D., & Davies, H. C. (1996). Surrogate climate-change sce-
 554 narios for regional climate models. *Geophysical Research Letters*, 23(6), 669-
 555 672.
- 556 Seneviratne, S. I., Zhang, X., Adnan, M., Badi, W., Dereczynski, C., Di Luca, A., ...
 557 Zhou, B. (2021). Weather and climate extreme events in a changing climate.
 558 in: *Climate change 2021: The physical science basis. contribution of work-*
 559 *ing group i to the sixth assessment report of the intergovernmental panel on*
 560 *climate change*. Cambridge University Press.
- 561 Shutts, G. (2005). A kinetic energy backscatter algorithm for use in ensemble predic-
 562 tion systems. *Quarterly Journal of the Royal Meteorological Society*, 131(612),
 563 3079-3102.
- 564 Skamarock, W. C., Klemp, J. B., Dudhia, J., Gill, D. O., Barker, D. M., Duda,
 565 M. G., ... Powers, J. G. (2008). A description of the advanced research wrf
 566 version 3. *NCAR Technical Note NCAR/TN-475+STR.*
- 567 Stone, D. A., Christidis, N., Folland, C., Perkins-Kirkpatrick, S., Perlwitz, J., Sh-
 568 iogama, H., ... Tadross, M. (2019). Experiment design of the International
 569 CLIVAR C20C+ Detection and Attribution project. *Weather and Climate*
 570 *Extremes*, 24, 100206. doi: <https://doi.org/10.1016/j.wace.2019.100206>
- 571 Stott, P. A., Christidis, N., Otto, F. E. L., Sun, Y., Vanderlinden, J.-P., van Olden-
 572 borgh, G. J., ... Zwiers, F. W. (2016). Attribution of extreme weather and
 573 climate-related events. *WIREs Climate Change*, 7(1), 23-41. Retrieved from
 574 <https://wires.onlinelibrary.wiley.com/doi/abs/10.1002/wcc.380> doi:
 575 <https://doi.org/10.1002/wcc.380>
- 576 Sumner, E. J. (1954). A study of blocking in the atlantic-european of the northern
 577 hemisphere. *Quarterly Journal of the Royal Meteorological Society*, 80(345),
 578 402-416.
- 579 Sun, Q., Miao, C., Hanel, M., Borthwick, A. G. L., Duan, Q., Ji, D., & Li, H.
 580 (2019). Global heat stress on health, wildfires, and agricultural crops under
 581 different levels of climate warming. *Environment International*, 128, 125-136.
- 582 van Oldenborgh, G. J., van der Wiel, K., Kew, S., Philip, S., Otto, F., Vautard, R.,
 583 ... van Aalst, M. (2021). Pathways and pitfalls in extreme event attribution.
 584 *Climatic Change*, 166(1), 13. Retrieved from [https://doi.org/10.1007/](https://doi.org/10.1007/s10584-021-03071-7)
 585 [s10584-021-03071-7](https://doi.org/10.1007/s10584-021-03071-7) doi: 10.1007/s10584-021-03071-7
- 586 van Oldenborgh, G. J., Wehner, M. F., Vautard, R., Otto, F. E. L., Seneviratne,
 587 S. I., Stott, P. A., ... Kew, S. F. (2022). Attributing and projecting heatwaves
 588 is hard: we can do better. *Earth's Future*, Submitted.
- 589 Vogel, M. M., Zscheischler, J., Fischer, E. M., & Seneviratne, S. I. (2020). Develop-
 590 ment of future heatwaves for different hazard thresholds. *Journal of Geophys-*
 591 *ical Research: Atmospheres*, 125(9), e2019JD032070. doi: [https://doi.org/10](https://doi.org/10.1029/2019JD032070)
 592 [.1029/2019JD032070](https://doi.org/10.1029/2019JD032070)
- 593 Wehner, M., Gleckler, P., & Lee, J. (2020). Characterization of long period re-
 594 turn values of extreme daily temperature and precipitation in the CMIP6
 595 models: Part 1, model evaluation. *Weather and Climate Extremes*, 100283.
 596 Retrieved from [http://www.sciencedirect.com/science/article/pii/](http://www.sciencedirect.com/science/article/pii/S2212094719302440)
 597 [S2212094719302440](http://www.sciencedirect.com/science/article/pii/S2212094719302440) doi: <https://doi.org/10.1016/j.wace.2020.100283>
- 598 Wehner, M., Stone, D., Shiogama, H., Wolski, P., Ciavarella, A., Christidis, N., &

- 599 Krishnan, H. (2018). Early 21st century anthropogenic changes in extremely
600 hot days as simulated by the C20C+ detection and attribution multi-model
601 ensemble. *Weather and Climate Extremes*, *20*, 1–8. Retrieved from [https://](https://www.sciencedirect.com/science/article/pii/S2212094717301159)
602 www.sciencedirect.com/science/article/pii/S2212094717301159 doi:
603 <https://doi.org/10.1016/j.wace.2018.03.001>
- 604 Wehner, M., Zarzycki, C., & Patricola, C. (2019). Estimating the human influ-
605 ence on tropical cyclone intensity as the climate changes. In J. Collins &
606 K. J. Walsh (Eds.), *Hurricane risk* (pp. 235–260). Springer.
- 607 Woollings, T., Barriopedro, D., Methven, J., Son, S.-W., Martius, O., Harvey, B., ...
608 Seneviratne, S. (2018). Blocking and its response to climate change. *Current*
609 *Climate Change Reports*, *4*(3), 287-300.
- 610 Wuebbles, D., Meehl, G., Hayhoe, K., Karl, T. R., Kunkel, K., Santer, B., ... Sun,
611 L. (2014). Cmp5 climate model analyses: Climate extremes in the united
612 states. *Bulletin of the American Meteorological Society*, *95*(4), 571-583.
- 613 Zhang, L., & Shaby, B. A. (2022). Reference priors for the generalized extreme value
614 distribution. *Statistica Sinica*. doi: <https://doi.org/10.5705/ss.202021.0258>

Supporting Information for “Anthropogenic contributions to the 2021 Pacific Northwest heatwave”

Emily Bercos-Hickey¹, Travis A. O’Brien^{2,1}, Michael F. Wehner¹, Likun Zhang^{3,1}, Christina M. Patricola^{4,1}, Huanping Huang¹, Mark D. Risser¹

¹Climate and Ecosystem Sciences Division, Lawrence Berkeley National Laboratory, Berkeley, California, USA

²Department of Earth and Atmospheric Sciences, Indiana University, Bloomington, Indiana, USA

³Department of Statistics, University of Missouri, Columbia, Missouri, USA

⁴Department of Geological and Atmospheric Sciences, Iowa State University, Ames, Iowa, USA

1. Non-stationary GEV analysis

The non-stationary generalized extreme value (GEV) analysis on individual station data uses a GEV distribution with a location parameter linearly dependent on a sum-total forcing variable for five well-mixed greenhouse gases (WMGHGs) to accommodate non-stationarity (Risser et al., 2021). The five WMGHGs include carbon dioxide, CFC-11 and CFC-12 halocarbons, methane and nitrous oxide, whose concentration values come from Meinshausen and Vogel (2016) and Meinshausen and Nicholls (2018) and whose forcing formulae can be found in Etminan, Myhre, Highwood, and Shine (2016) and Hodnebrog et al. (2013). To estimate the GEV parameters, we impose a non-informative

16 prior on the shape parameter (Zhang & Shaby, 2022), and then run a Metropolis-Hastings
17 algorithm to draw samples from the posterior distributions of the parameters. Since the
18 GEV distribution has a finite upper bound when the shape parameter is negative, we can
19 directly examine the posterior distribution of the upper bound.

2. Configuration of the Weather Research and Forecast (WRF) model

20 Some simulations of the PNW heatwave in this study were performed using the Weather
21 Research and Forecasting (WRF) model (Skamarock et al., 2008) version 3.8.1. Model
22 output was generated every hour with 50 vertical levels from a grid with horizontal spac-
23 ings of either 18 km or 50 km. The WRF simulation domains are shown in Figure S2a.
24 Parameterization schemes used in all simulations include: the Rapid Radiative Transfer
25 Model for Global Climate Models (Iacono et al., 2008) short and longwave schemes, the
26 WRF single-moment 6-class microphysics scheme (Hong & Lim, 2006), the Noah land sur-
27 face model scheme (Chen & Dudhia, 2001), the Medium Range Forecast (MRF) boundary
28 layer scheme (Hong & Pan, 1996), and the Grell-Freitas ensemble cumulus scheme (Grell
29 & Freitas, 2014). Ten-member ensembles at both grid spacings were generated using
30 the Stochastic Kinetic Energy Backscatter Scheme (SKEBS) (Shutts, 2005; Berner et al.,
31 2011). SKEBS uses random stream function perturbations to represent model uncertainty
32 from unresolved scales and has previously been used to generate WRF ensembles (Berner
33 et al., 2011; Patricola & Wehner, 2018). The daily maximum temperature and geopoten-
34 tial height contours at 500 hPa on June 28, 2021 are shown for the ten ensemble members
35 at 18 km and the ensemble average in Figure S3.

3. Configuration of the International Centre for Theoretical Physics Regional Climate Model (RegCM)

Some simulations of the PNW heatwave in this study were performed using the International Centre for Theoretical Physics RegCM4 regional model (Giorgi et al., 2012). The simulations were configured with 18 km and 50 km horizontal grid spacings and 30 sigma levels with a model top pressure of 50 hPa, a timestep of 36 seconds, and model output saved every 3 hours. The RegCM simulation domains are shown in Fig. S2b. The simulations used hydrostatic dynamics, the National Center for Atmospheric Research (NCAR) Community Climate Model 3 radiation parameterization (Kiehl et al., 1996), the University of Washington turbulence closure and planetary boundary layer parameterization (Grenier & Bretherton, 2001; O'Brien et al., 2012), the Massachusetts Institute of Technology convection parameterization (Emanuel, 1991; Emanuel & Živković-Rothman, 1999), and the Biosphere Atmosphere Transfer Scheme 1e (Dickinson et al., 1993). Ensemble simulations at 18 km and 50 km resolution were generated by perturbing the initial and boundary condition temperature field by 0.1% (O'Brien et al., 2011). The daily maximum temperature and geopotential height contours at 500 hPa on June 28, 2021 are shown for the ten ensemble members at 18 km and the ensemble average in Figure S4.

The RegCM 4.9.5 simulations are based on the master branch of the github code at commit 8197f9, with an additional bug fix applied that allows the code to run at the National Energy Research Supercomputing Center (NERSC). (This bug fix was merged with the master branch of the code in commit 6b43573.)

4. Model Validation

55 To establish the validity of the heatwave simulations, we compare the WRF and RegCM
56 hindcasts, the datasets that provided their initial and boundary conditions (ICBCs),
57 NARR and GFS, respectively, and the GHCN observational data. Figure 3a shows the
58 June 25-July 1, 2021 daily maximum temperature averaged over the region 45°N - 52°N and
59 124°W - 119°W (Figure S2) from the GHCN (black), ensemble-averaged WRF historical
60 simulations (blue, solid), NARR (blue, dashed), ensemble-averaged RegCM historical sim-
61 ulations (red, solid), and GFS (red, dashed). The shading around the WRF and RegCM
62 lines show the range of values from the 10-member ensembles. From Figure 3a, the NARR
63 and GFS are over 6°C cooler than the GHCN and about a day late in reaching the hottest
64 temperatures. The timing and magnitude of the daily maximum temperatures through-
65 out the heatwave from the WRF and RegCM models are mostly in close alignment with
66 the NARR and GFS, respectively. The differences between the WRF and the NARR and
67 the RegCM and the GFS seen in Figure 3a are not surprising and are likely due to the
68 models departing from their initial conditions and the chosen parameterization schemes.
69 Although both models and the data used for their ICBCs produce a cooler and delayed
70 heatwave, WRF and RegCM are consistent with each other in their simulations of the
71 heatwave event despite using different ICBCs and parameterizations.

72 To further examine the validity of the WRF and RegCM hindcasts, we compare the
73 models with the European Centre for Medium-range Weather Forecasts (ECMWF) re-
74 analysis five (ERA5) (Hersbach et al., 2020) on June 28, 2021, the hottest day of the
75 heatwave from the GHCN (Figure 3a). Figure S5 shows the daily maximum temperature
76 and 500 hPa height contours from (a) the ERA5, (b) the ensemble-averaged WRF his-

77 torical simulations, and (c) the ensemble-averaged RegCM historical simulations. Figure
78 S5a shows the high temperatures and omega blocking pattern that were distinct features
79 of the PNW heatwave. Figures S5b,c show that the WRF and RegCM models are cor-
80 rectly replicating the key features of the heatwave, thus lending confidence to the hindcast
81 simulations.

82 Lastly, we examine how the horizontal spatial resolution may affect the hindcast sim-
83 ulations. The effects of resolution on the WRF and RegCM simulations can be seen in
84 Fig. S6, which shows the June 25-July 1, 2021 time series of the spatially averaged (see
85 Figure S2) daily maximum temperature from the GHCN, NARR, GFS, and the ensemble
86 averages of the 18 km and 50 km WRF and RegCM historical simulations. For the WRF
87 model, Figure S6 shows that there is little difference between the daily maximum tem-
88 perature at 18 km and 50 km. For the RegCM model, Figure S6 indicates that the daily
89 maximum temperature is similar between the two resolutions, with a notable exception
90 on June 29 where it is cooler at 18 km than at 50 km.

91 Figures S7 and S8 show the daily maximum temperature and geopotential height con-
92 tours at 500 hPa on June 28, the hottest day of the heatwave according to the GHCN
93 (Figure S6), for the ten ensemble members and the ensemble average from the 50 km
94 historical simulations of the WRF and RegCM models, respectively. A comparison of
95 Figures S3 and S7 reveals that the WRF model simulates the omega blocking pattern and
96 high temperatures of the heatwave at both resolutions. Similarly, a comparison of Figures
97 S4 and S8 indicates the the RegCM model also simulates the omega blocking pattern and
98 high temperatures at both resolutions.

99 To visualize the differences between the 18 km and 50 km resolution simulations, Figure
100 S9 shows the ensemble average of the daily maximum temperature on June 28 from the
101 (a) 18 km WRF, (b) 50 km WRF, (d) 18 km RegCM, and (e) 50 km RegCM historical
102 simulations. The difference between the daily maximum temperature in the 18 km and
103 50 km ensemble averages is shown for the (c) WRF and (f) RegCM models. From Figure
104 S9a,b, the WRF model is capturing the high temperatures associated with the heatwave
105 event at both resolutions. Figure S9c indicates that, for most of the region affected by
106 the heatwave, the 18 km simulations are 0-2°C warmer than the 50 km simulations. From
107 Figure S9d,e, the RegCM model is mostly capturing the high temperatures associated
108 with the heatwave, although temperatures in eastern Washington are notably lower in the
109 50 km simulations. In contrast to the WRF model, the difference between the RegCM
110 18 km and 50 km simulations (Figure S9f) shows large positive and negative anomalies
111 throughout the domain. The anomalies in Figure S9f are likely due to the elevation
112 differences between the two resolutions, where the 50 km simulations will not resolve
113 terrain as well as the 18 km simulations. The 50 km simulations are therefore warmer in
114 higher elevation regions such as the North Cascades and the Sierra Nevada Mountains.
115 Although the choice of resolution does not strongly affect the ability of the WRF and
116 RegCM models to capture the overall characteristics of the PNW heatwave (see Figures
117 S3, S7, S4, and S8), due to the elevation bias present in the 50 km simulations, we use
118 the 18 km WRF and RegCM simulations for the remainder of the analysis.

5. Pseudo-global warming (PGW) / Hindcast Attribution methodology

119 The PGW Hindcast Attribution method assumes that similar synoptic conditions,
120 mainly the omega block and atmospheric river, that produced the PNW heatwave in
121 the historical time period could happen in past and future climates. This is a restrictive
122 assumption, precluding any statement about how the frequency of such large scale con-
123 ditions will change. The variables adjusted in the WRF initial and boundary conditions
124 include temperature, relative humidity, geopotential height, sea-level and surface pres-
125 sure, sea-surface temperature, and surface temperature; for RegCM, only the temperature
126 and specific humidity fields were altered. Additionally, we modified the WRF radiation
127 code to account for different greenhouse gas concentrations of CO₂, CH₄, N₂O, CFC-11,
128 CFC-12 and CCl₄ in the counterfactual climate simulations consistent with pre-industrial
129 and Shared Socioeconomic Pathway 585 (SSP585) (O'Neill et al., 2016) specifications
130 (Meinshausen & Vogel, 2016). Greenhouse gas concentrations were modified in RegCM
131 using built in tables for the year 1850 and for the year 2090 under the SSP585.

132 The PGW deltas were calculated from the Coupled Model Intercomparison Project
133 Phase 6 (CMIP6) (Danabasoglu, 2019) data by computing a multi-model average (Table
134 S1) and subtracting the 1995-2014 averaged historical simulations from: 1) The averaged
135 hist-nat simulations; 2) The 2040-2060 averaged SSP585 simulations (mid-century); and
136 3) The 2080-2100 averaged SSP585 simulations (late-century). The length of the his-
137 torical timeframe was chosen to capture the historical climate and to smooth out any
138 multi-decadal variability. The hist-nat simulation resembles the historical simulation but
139 only includes solar and volcanic forcing (Eyring et al., 2016) and the SSP585 simulation
140 incorporates future emissions and land use changes (O'Neill et al., 2016). Deltas were

141 calculated for the month of the heatwave event and were added to the corresponding ini-
142 tial and boundary conditions. Hist-nat, mid-century, and late-century simulations were
143 performed with the WRF model, and only nat-hist and late-century simulations were
144 performed with the RegCM model.

References

- 145 Berner, J., Ha, S.-Y., Hacker, J. P., Fournier, A., & Snyder, C. (2011). Model un-
146 certainty in a mesoscale ensemble prediction system: Stochastic versus multiphysics
147 representations. *Monthly Weather Review*, *139*(6), 1972-1995.
- 148 Chen, F., & Dudhia, J. (2001). Coupling an advanced land surface–hydrology model
149 with the penn state–ncar mm5 modeling system. part i: Model implementation and
150 sensitivity. *Monthly Weather Review*, *129*(4), 569-585.
- 151 Danabasoglu, G. (2019). *NCAR CESM2 model output prepared for CMIP6 CMIP*.
152 Earth System Grid Federation. Retrieved from [https://doi.org/10.22033/ESGF/](https://doi.org/10.22033/ESGF/CMIP6.2185)
153 [CMIP6.2185](https://doi.org/10.22033/ESGF/CMIP6.2185) doi: 10.22033/ESGF/CMIP6.2185
- 154 Dickinson, R. E., Henderson-Sellers, A., Kennedy, P. J., & Wilson, M. F. (1993).
155 Biosphere atmosphere transfer scheme (BATS) version 1e as coupled for Commu-
156 nity Climate Model. *NCAR Tech. Note NCAR/TN-378+SR*(August), 77. doi:
157 [10.1029/2009JD012049](https://doi.org/10.1029/2009JD012049)
- 158 Emanuel, K. A. (1991, nov). A Scheme for Representing Cumulus Convection in
159 Large-Scale Models. *Journal of the Atmospheric Sciences*, *48*(21), 2313–2329. Re-
160 trieved from [http://journals.ametsoc.org/doi/10.1175/1520-0469\(1991\)048%](http://journals.ametsoc.org/doi/10.1175/1520-0469(1991)048%3C2313:ASFRCC%3E2.0.CO;2)
161 [3C2313:ASFRCC%3E2.0.CO;2](http://journals.ametsoc.org/doi/10.1175/1520-0469(1991)048%3C2313:ASFRCC%3E2.0.CO;2) doi: 10.1175/1520-0469(1991)048(2313:ASFRCC)2.0

.CO;2

Emanuel, K. A., & Živković-Rothman, M. (1999, jun). Development and Evaluation of a Convection Scheme for Use in Climate Models. *Journal of the Atmospheric Sciences*, 56(11), 1766–1782. Retrieved from [http://journals.ametsoc.org/doi/10.1175/1520-0469\(1999\)056%3C1766:DAEOAC%3E2.0.CO;2](http://journals.ametsoc.org/doi/10.1175/1520-0469(1999)056%3C1766:DAEOAC%3E2.0.CO;2) doi: 10.1175/1520-0469(1999)056<1766:DAEOAC>2.0.CO;2

Etminan, M., Myhre, G., Highwood, E., & Shine, K. (2016). Radiative forcing of carbon dioxide, methane, and nitrous oxide: A significant revision of the methane radiative forcing. *Geophysical Research Letters*, 43(24), 12–614.

Eyring, V., Bony, S., Meehl, G. A., Senior, C. A., Stevens, B., Stouffer, R. J., & Taylor, K. E. (2016). Overview of the coupled model intercomparison project phase 6 (cmip6) experimental design and organization. *Geosci. Model Dev.*, 9(5), 1937-1958. doi: 10.5194/gmd-9-1937-2016

Giorgi, F., Coppola, E., Solmon, F., Mariotti, L., Sylla, M., Bi, X., ... Brankovic, C. (2012). RegCM4: model description and preliminary tests over multiple CORDEX domains. *Climate Research*, 52, 7–29. Retrieved from <http://www.int-res.com/abstracts/cr/v52/p7-29/> doi: 10.3354/cr01018

Grell, G. A., & Freitas, S. R. (2014). A scale and aerosol aware stochastic convective parameterization for weather and air quality modeling. *Atmos. Chem. Phys.*, 14(10), 5233-5250.

Grenier, H., & Bretherton, C. S. (2001). A Moist PBL Parameterization for Large-Scale Models and Its Application to Subtropical Cloud-Topped Marine Boundary Layers.

- 184 *Monthly Weather Review*, 129(3), 357–377. Retrieved from [http://dx.doi.org/](http://dx.doi.org/10.1175/1520-0493(2001)129%3C0357:AMPPFL%3E2.0.CO%5Cn2)
185 10.1175/1520-0493(2001)129%3C0357:AMPPFL%3E2.0.CO%5Cn2 doi: 10.1175/1520
186 -0493(2001)129<0357:AMPPFL>2.0.CO;2
- 187 Hersbach, H., Bell, B., Berrisford, P., Hirahara, S., Horányi, A., Muñoz-Sabater, J.,
188 ... others (2020). The era5 global reanalysis. *Quarterly Journal of the Royal*
189 *Meteorological Society*, 146(730), 1999–2049.
- 190 Hodnebrog, Ø., Etminan, M., Fuglestvedt, J., Marston, G., Myhre, G., Nielsen, C., ...
191 Wallington, T. (2013). Global warming potentials and radiative efficiencies of halo-
192 carbons and related compounds: A comprehensive review. *Reviews of Geophysics*,
193 51(2), 300–378.
- 194 Hong, S.-Y., & Lim, J.-O. J. (2006). The wrf single-moment 6-class microphysics scheme
195 (wsm6). *Journal of the Korean Meteorological Society*, 42(2), 129-151.
- 196 Hong, S.-Y., & Pan, H.-L. (1996). Nonlocal boundary layer vertical diffusion in a medium-
197 range forecast model. *Monthly Weather Review*, 124(10), 2322-2339.
- 198 Iacono, M. J., Delamere, J. S., Mlawer, E. J., Shephard, M. W., Clough, S. A., & Collins,
199 W. D. (2008). Radiative forcing by long-lived greenhouse gases: Calculations with the
200 aer radiative transfer models. *Journal of Geophysical Research*, 113(D13), D13103.
- 201 Kiehl, J., Hack, J., Bonan, G., Boville, B., Briegleb, B., Williamson, D., & Rasch, P.
202 (1996). *Description of the NCAR Community Climate Model (CCM3)* (Tech. Rep.
203 No. September). doi: 10.5065/D6FF3Q99
- 204 Meinshausen, M., & Nicholls, Z. R. J. (2018). *Uom-remind-magpie-ssp585-1-2-0:*
205 *Remind-magpie-ssp585 ghg concentrations*. Earth System Grid Federation. Retrieved

from <https://doi.org/10.22033/ESGF/input4MIPs.2349> doi: 10.22033/ESGF/
input4MIPs.2349

Meinshausen, M., & Vogel, E. (2016). input4mips.uom.ghgconcentrations.cmip.uom-
cmip-1-2-0. *Earth System Grid Federation*. doi: 10.22033/ESGF/input4MIPs.1118

O'Brien, T. A., Chuang, P. Y., Sloan, L. C., Faloon, I. C., & Rossiter, D. L. (2012).
Coupling a new turbulence parametrization to RegCM adds realistic stratocumulus
clouds. *Geoscientific Model Development*, 5(4), 989–1008. doi: 10.5194/gmd-5-989
-2012

O'Brien, T. A., Sloan, L. C., & Snyder, M. A. (2011, sep). Can ensembles of regional
climate model simulations improve results from sensitivity studies? *Climate Dy-
namics*, 37(5-6), 1111–1118. Retrieved from [http://link.springer.com/10.1007/
s00382-010-0900-5](http://link.springer.com/10.1007/s00382-010-0900-5) doi: 10.1007/s00382-010-0900-5

O'Neill, B. C., Tebaldi, C., Van Vuuren, D. P., Eyring, V., Friedlingstein, P., Hurtt,
G., ... Sanderson, B. M. (2016). The Scenario Model Intercomparison Project
(ScenarioMIP) for CMIP6. *Geoscientific Model Development*, 9(9), 3461–3482. doi:
10.5194/gmd-9-3461-2016

Patricola, C. M., & Wehner, M. F. (2018). Anthropogenic influences on major tropical
cyclone events. *Nature*, 563(7731), 339-346.

Risser, M., Wehner, M., O'Brien, J., Patricola, C., O'Brien, T., Collins, W., ... Huang,
H. (2021). Quantifying the influence of natural climate variability on in situ mea-
surements of seasonal total and extreme daily precipitation. *Climate Dynamics*. doi:
10.1007/s00382-021-05638-7

- 228 Shutts, G. (2005). A kinetic energy backscatter algorithm for use in ensemble prediction
229 systems. *Quarterly Journal of the Royal Meteorological Society*, 131 (612), 3079-3102.
- 230 Skamarock, W. C., Klemp, J. B., Dudhia, J., Gill, D. O., Barker, D. M., Duda, M. G., ...
231 Powers, J. G. (2008). A description of the advanced research wrf version 3. *NCAR*
232 *Technical Note NCAR/TN-475+STR..*
- 233 Zhang, L., & Shaby, B. A. (2022). Reference priors for the generalized extreme value
234 distribution. *Statistica Sinica*. doi: <https://doi.org/10.5705/ss.202021.0258>

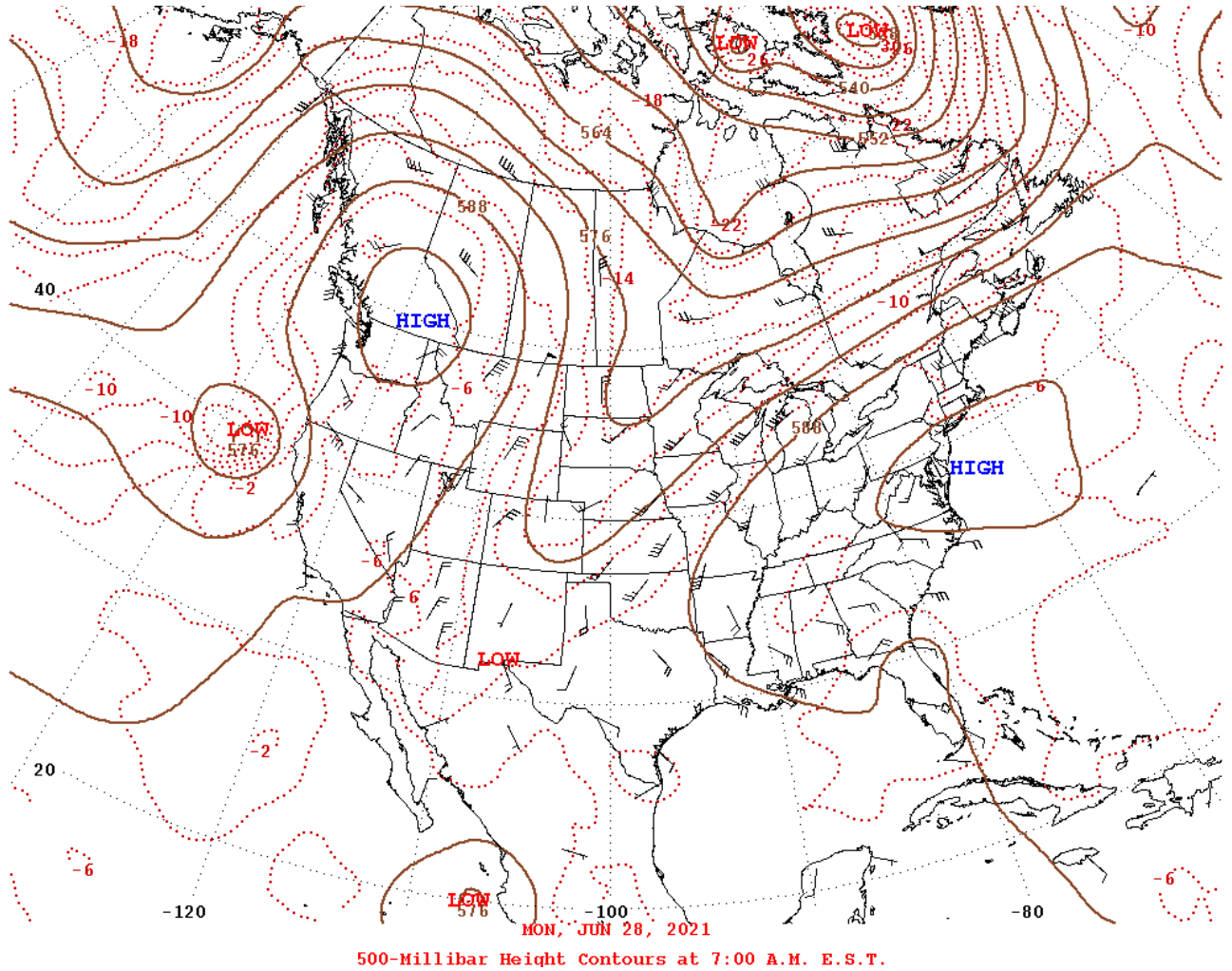


Figure S1. National Oceanic and Atmospheric Administration (NOAA) National Centers for Environmental Prediction (NCEP) 500 hPa height contours on June 28, 2021.

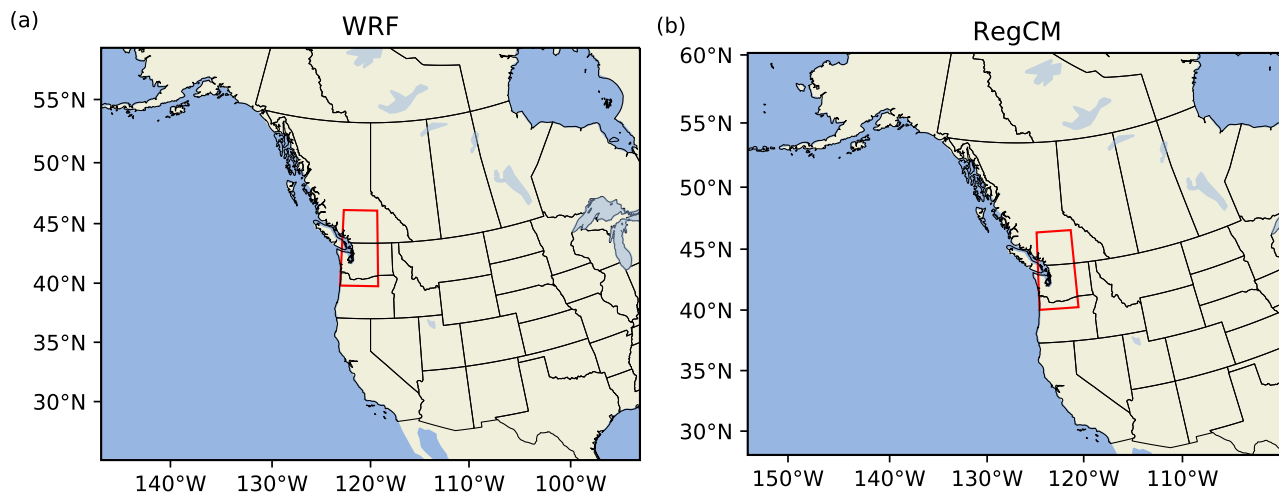


Figure S2. Simulation domains for the (a) WRF model, and (b) RegCM. The red boxes show the region 45°N-52°N and 124°W-119°W, which is used for spatial averaging and is common to both models.

Table S1. CMIP6 models used to calculate the multi-model averaged deltas used in the pseudo-global warming method.

Model
ACCESS-CM2
ACCESS-ESM1-5
CESM2
CNRM-CM6-1
CanESM5
FGOALS-g3
GFDL-CM4
GFDL-ESM4
GISS-E2-1-G
HadGEM3-GC31-LL
IPSL-CM6A-LR
MIROC6
MRI-ESM2-0
NorESM2-LM

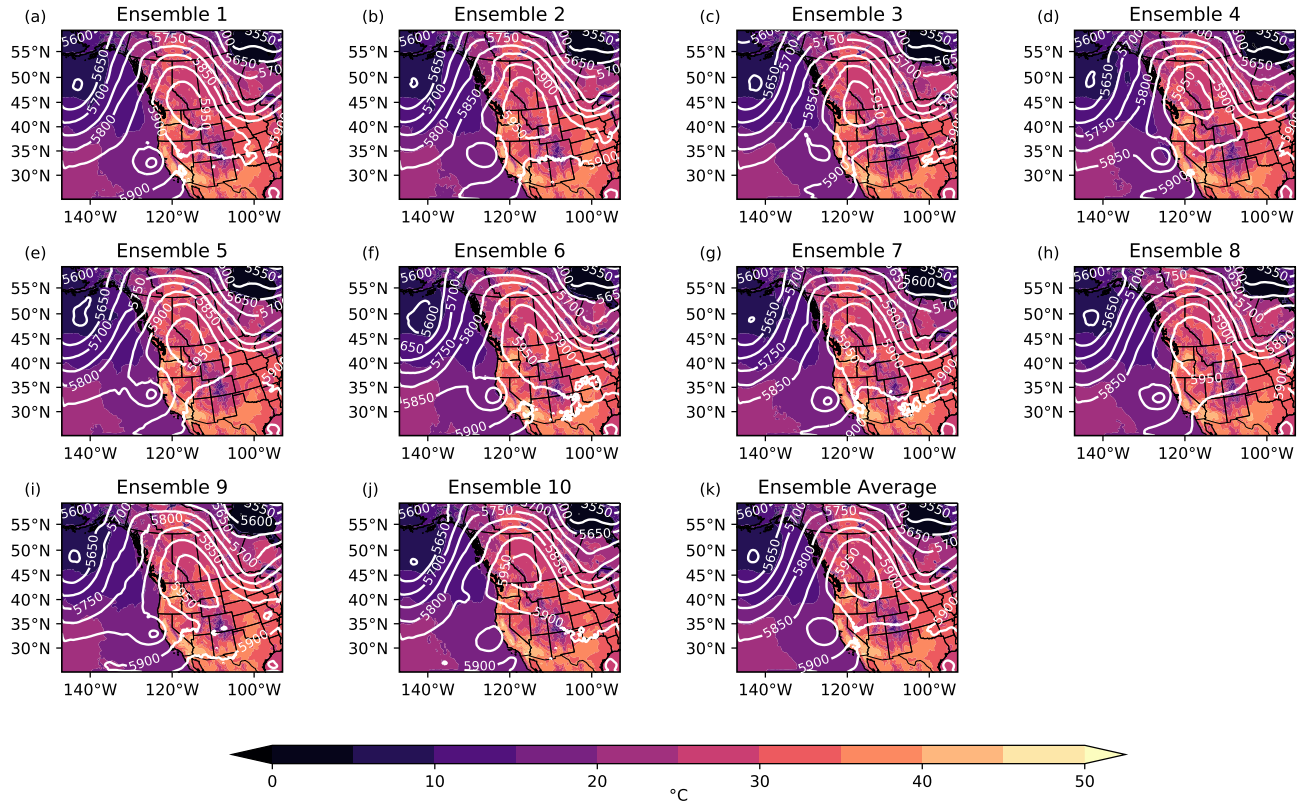


Figure S3. Historical 18 km WRF simulation (a)-(j) individual ensemble members and (k) ensemble-average of the daily maximum 2 m temperature ($^{\circ}\text{C}$; color contours) and geopotential height at 500 hPa and 0000 UTC (m; white contour lines) on June 28, 2021.

Table S2. Summary of model experiments, where an X indicates that an experiment was performed for the given model.

Experiments	WRF 18km	WRF 50km	RegCM 18km	RegCM 50km
Historical	X	X	X	X
Hist-nat	X	X	X	X
Mid-century	X	X		
Late-century	X	X	X	X
Hist-nat with soil moisture delta	X			
Mid-century with soil moisture delta	X			
Late-century with soil moisture delta	X			

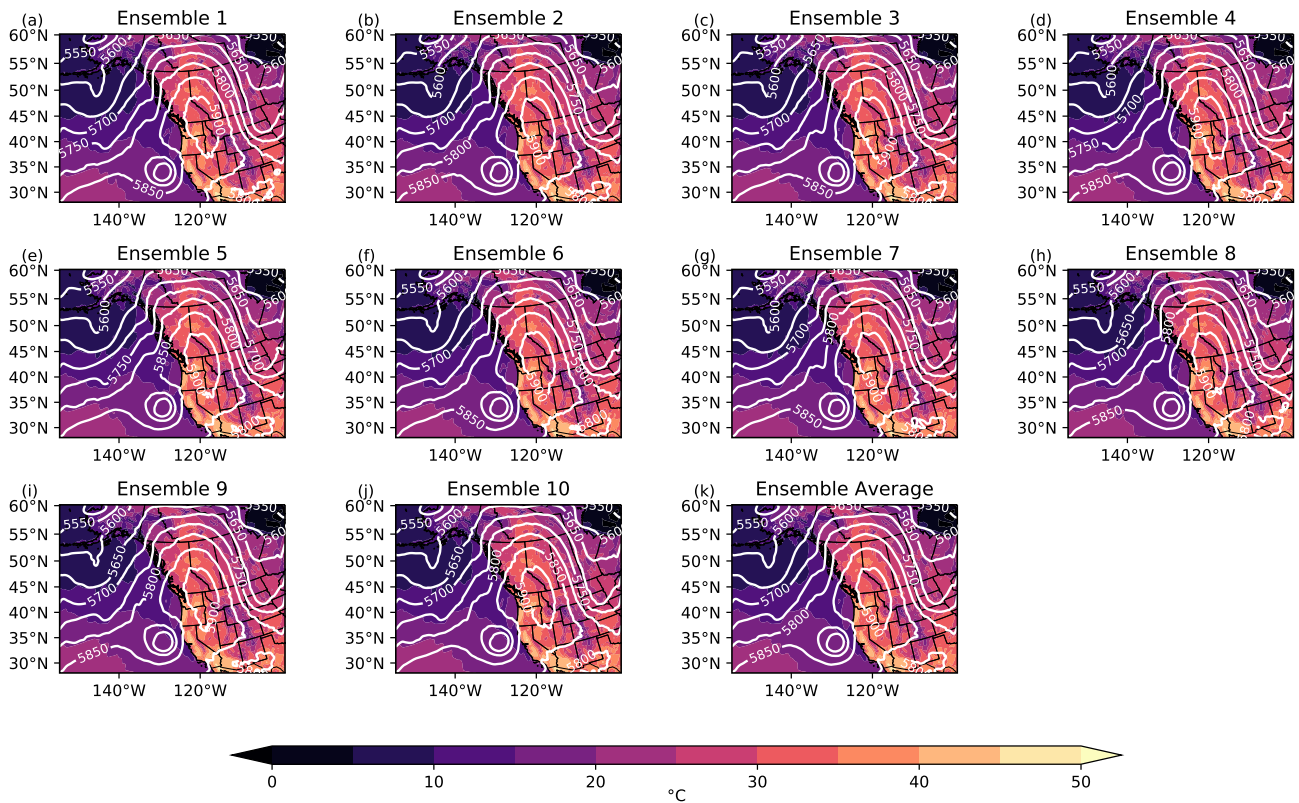


Figure S4. Historical 18 km RegCM simulation (a)-(j) individual ensemble members and (k) ensemble-average of the daily maximum 2 m temperature ($^{\circ}\text{C}$; color contours) and geopotential height at 500 hPa and 0000 UTC (m; white contour lines) on June 28, 2021.

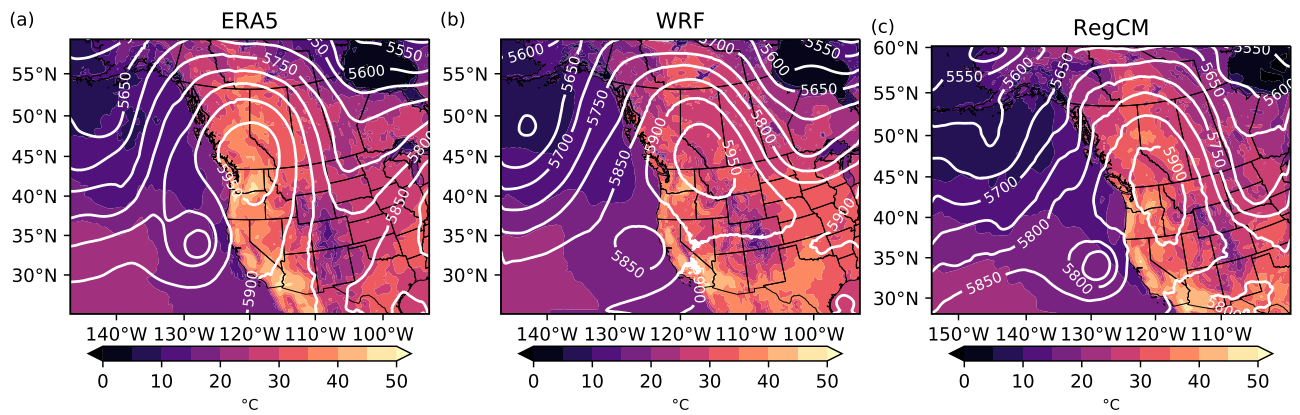


Figure S5. June 28, 2021 (a) ERA5, (b) WRF 18 km historical ensemble average, and (c) RegCM 18 km historical ensemble average of the daily maximum 2 m temperature (°C; color contours) and geopotential height at 500 hPa and 0000 UTC (m; white contour lines).

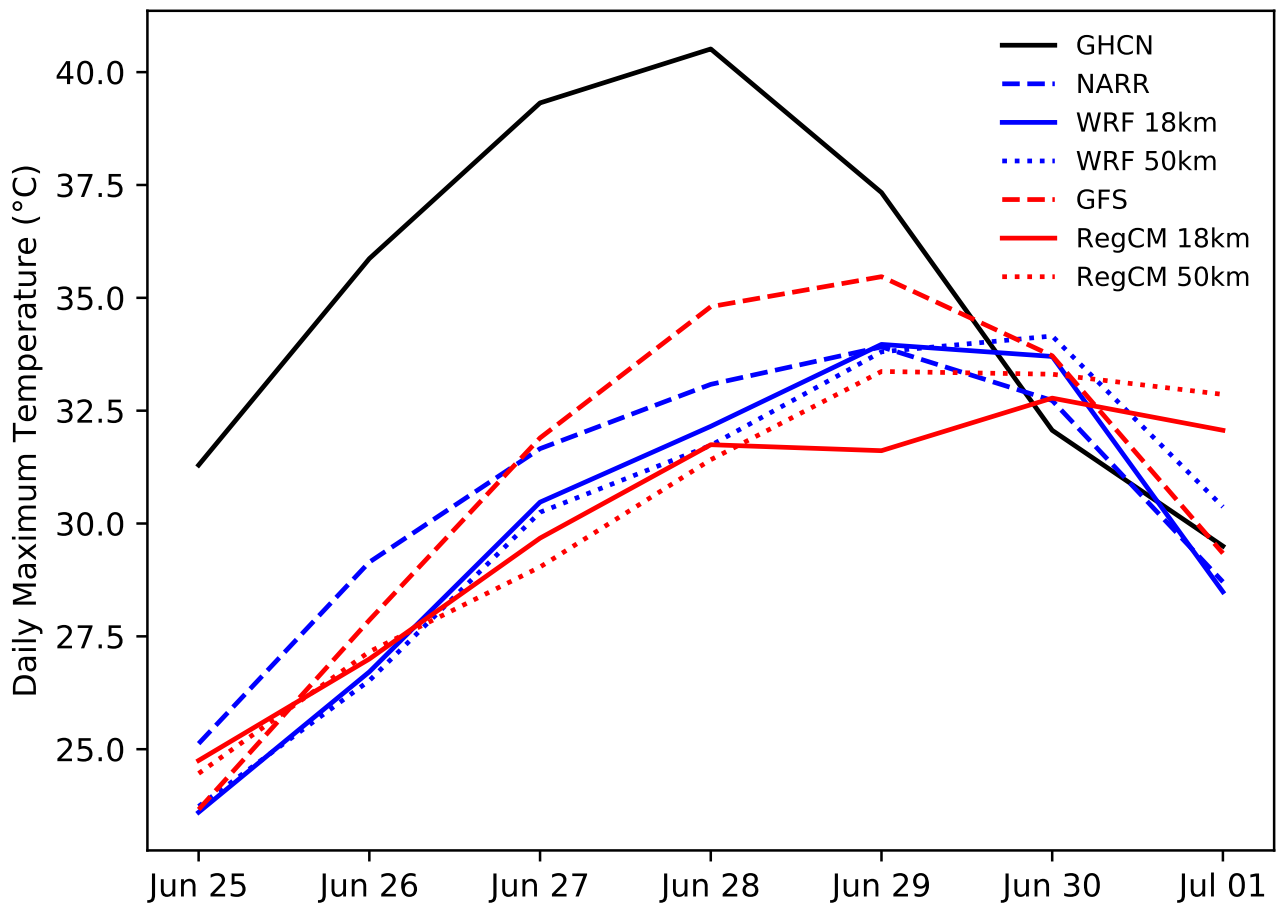


Figure S6. Time series from June 25-July 1, 2021 of the spatially averaged daily maximum temperature from the GHCN (black), NARR (blue, dashed), GFS (red, dashed), the 18 km WRF (blue, solid) and RegCM (red, solid) historical ensemble averages, and the 50 km WRF (blue, dotted) and RegCM (red, dotted) historical ensemble averages.

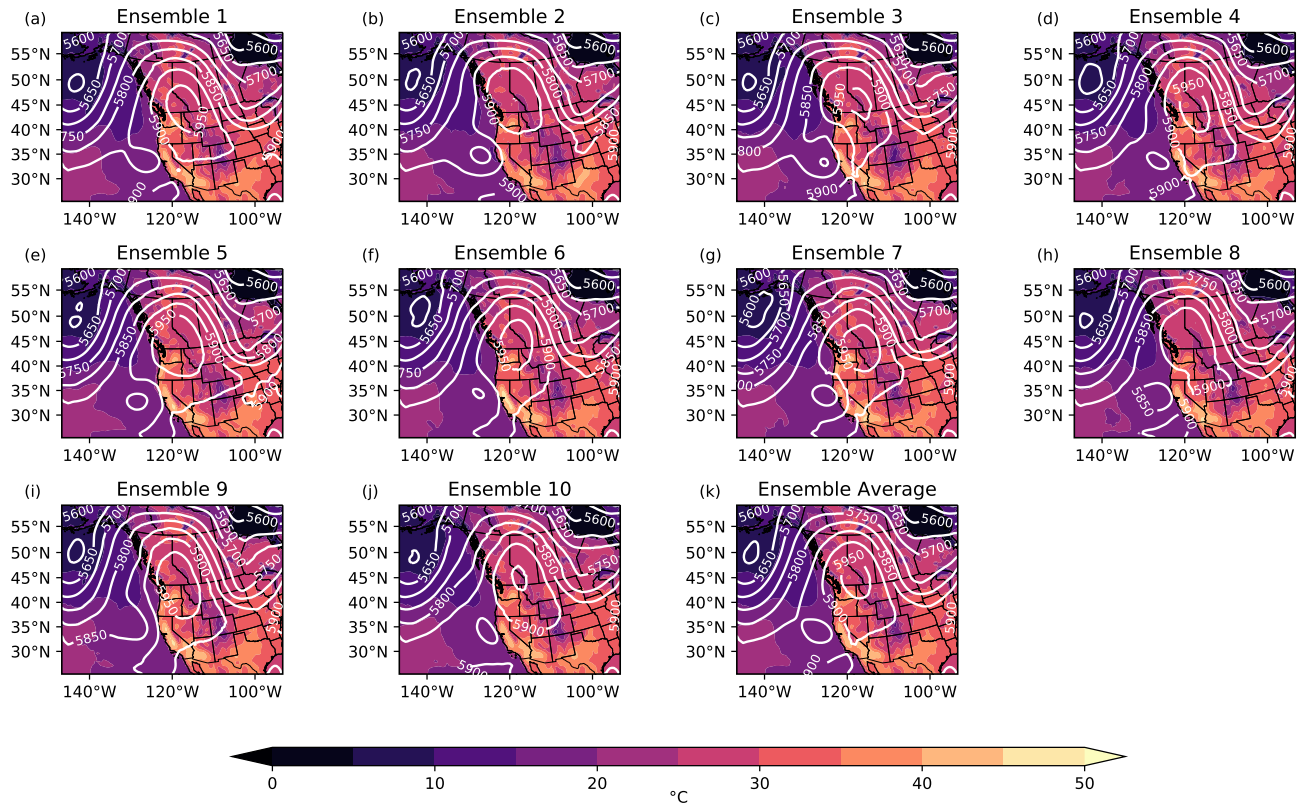


Figure S7. Historical 50 km WRF simulation (a)-(j) individual ensemble members and (k) ensemble-average of the daily maximum 2 m temperature ($^{\circ}\text{C}$; color contours) and geopotential height at 500 hPa and 0000 UTC (m; white contour lines) on June 28, 2021.

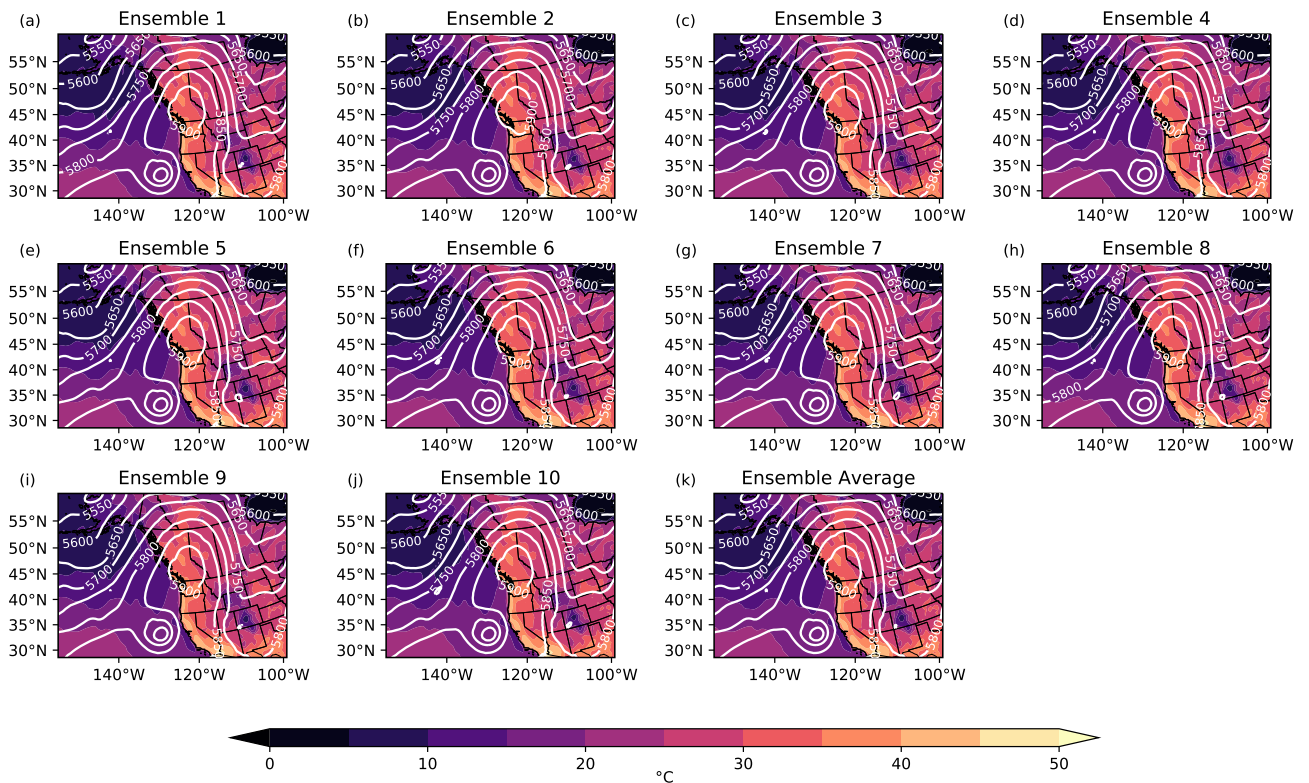


Figure S8. Historical 50 km RegCM simulation (a)-(j) individual ensemble members and (k) ensemble-average of the daily maximum 2 m temperature ($^{\circ}\text{C}$; color contours) and geopotential height at 500 hPa and 0000 UTC (m; white contour lines) on June 28, 2021.

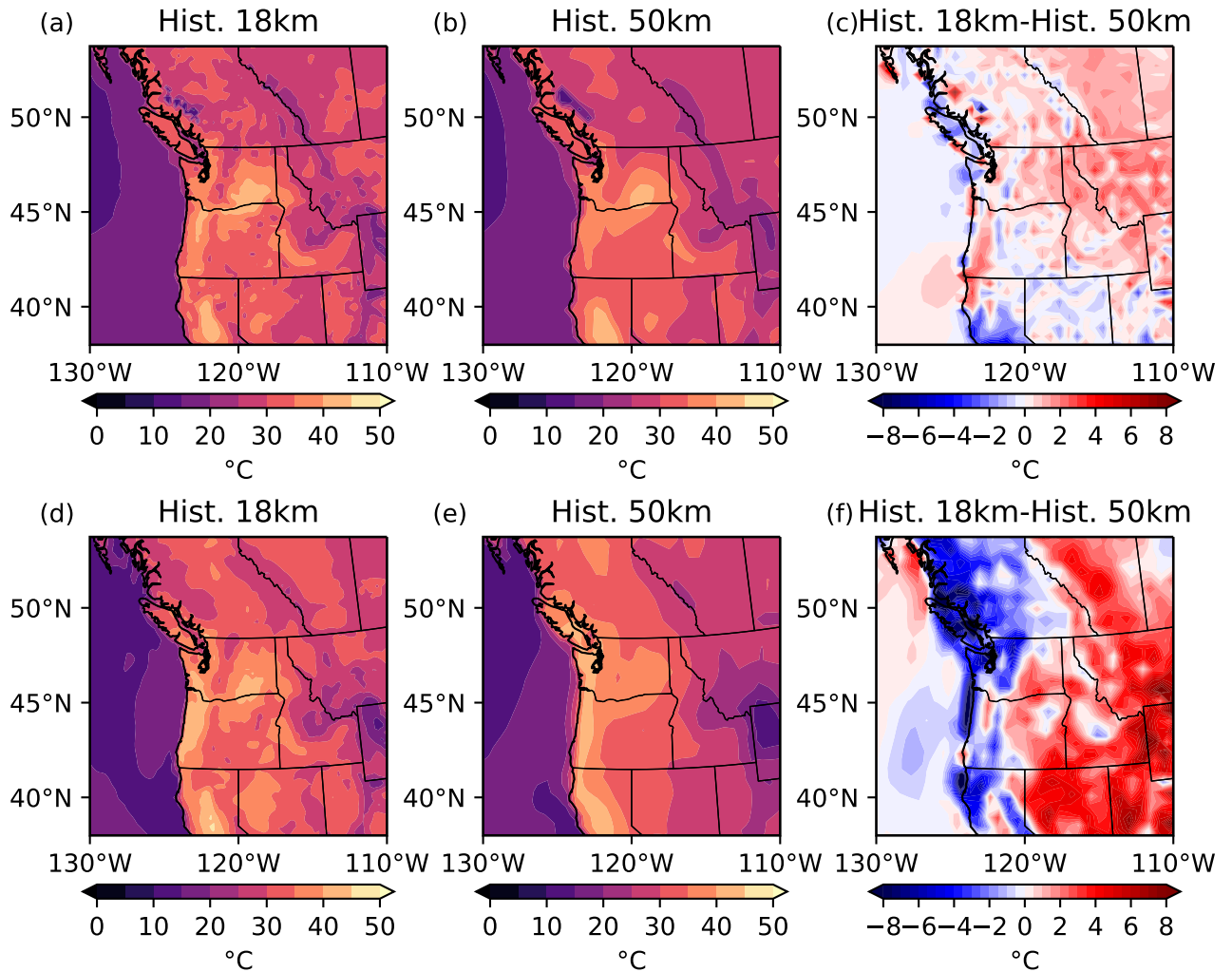


Figure S9. Historical ensemble-averaged daily maximum 2 m temperature (°C; color contours) from WRF at (a) 18 km, (b) 50 km, and (c) 18 km minus 50 km, and RegCM at (d) 18 km, (e) 50 km, and (f) 18 km minus 50 km on June 28, 2021.